

# **Study on Bond Degradation of Rebars in Cracked Concrete due to Bar Corrosion**

**SYLL AMADOU SAKHIR**

(Master's Program in Engineering Mechanics and Energy )

Advised by Kanakubo Toshiyuki

Submitted to the Graduate School of  
Systems and Information Engineering  
in Partial Fulfillment of the Requirements  
for the Degree of Master of Engineering  
at the  
University of Tsukuba

March 2020

## ABSTRACT

This study aims to quantify the bond strength of reinforcing bars in cracked concrete. It focuses on the more fundamental effect of the cracking itself (in absence of corrosion products). To achieve this aim, the simulation of the cracking of concrete due to corrosion of reinforcing bars by using an aluminum pipe embedded in concrete and filled with an expansion agent was proposed as a novel method. With the increase of the crack width over elapsed time from the filling of the expansion agent, a target crack width was obtained. The splitting cracks play a fundamental role in reducing the bond, therefore two cases were set: “Single-split type” when the splitting cracks are parallel or along the rebar and “Side split-type” when the splitting cracks are perpendicular to the rebar.

Following to tension test of the ribbed aluminum pipe, pull-out test was conducted on 28 specimens divided into two categories as described above. In this study, the induced crack width was taken as the main variable to find its influence on bond degradation.

These experiments confirmed that the expansion agent filled pipe is a promising method that allows focusing on the cracking itself. The tensile test also shows that the strain in the axis, top and between the ribs tended to increase over the time after the filling of the expansion agent. In addition, at the beginning of the loading, with the increasing of the axial strain, the yield strength and modulus of elasticity of the pipe filled with an expansion agent also increase. However, the elongation at failure tended to decrease. The tensile strength was not affected.

In pull-out test, all specimens experienced failure due to splitting. A group of specimens failed by newly generated splitting crack despite existing induced crack and other specimens failed by the opening of induced crack that the pull-out strength load reduces exponentially with the increase of crack width and this demonstrates that the surface crack width can potentially be a good indicator to evaluate the bond strength degradation. The research has also shown that the decrease of the pull-out strength is more severe in 18MPa specimens than in 30 MPa specimens. In addition, the deterioration of the bond due to the induced cracks was more severe in a “Side-split type” than in “Single split-type”.

**Keywords:** Concrete crack width, Rebar corrosion, Crack width, Expansion agent, Bond test, Deterioration of bond strength

## *Table of Contents*

**Study on Bond Degradation of Rebars in Cracked Concrete due to Bar Corrosion..**

**鉄筋腐食によりひび割れが生じたコンクリート中の鉄筋の付着劣化に関する研究**

<b>ABSTRACT .....</b>	<b>1</b>
<b>List of Figures .....</b>	<b>4</b>
<b>List of Tables .....</b>	<b>5</b>
<b>Chapter 1 Introduction .....</b>	<b>6</b>
<b>1.1. Background .....</b>	<b>6</b>
<b>1.2. Objectives of this study.....</b>	<b>8</b>
<b>1.3. Methodology of this study .....</b>	<b>8</b>
<b>1.4. Outline of the thesis .....</b>	<b>11</b>
<b>Chapter 2 Tensile properties of ribbed aluminum pipe filled with an expansion agent</b>	<b>12</b>
<b>2.1. Introduction.....</b>	<b>12</b>
<b>2.2. Background of crack simulation by aluminum pipe filled with an expansion agent</b>	<b>12</b>
<b>2.3. Experiment outline.....</b>	<b>13</b>
<b>2.3.1. Specimen Overview .....</b>	<b>13</b>
<b>2.3.2. Loading and Measurement.....</b>	<b>15</b>
<b>2.4. Experiment results .....</b>	<b>16</b>
<b>2.4.1. Strain before loading due to the expansion agent .....</b>	<b>16</b>
<b>2.4.2. Tensile test results .....</b>	<b>18</b>
<b>2.5. Conclusions.....</b>	<b>21</b>
<b>Chapter 3 Bond Degradation of Rebars in Cracked Concrete due to BAR: Single Splitting Case .....</b>	<b>22</b>
<b>3.1. Introduction.....</b>	<b>22</b>
<b>3.2. Experiment outline.....</b>	<b>22</b>
<b>3.2.1. Aluminum pipe with ribs .....</b>	<b>22</b>
<b>3.2.2. Pull-out specimen .....</b>	<b>22</b>
<b>3.2.3. Crack simulation by EAFP.....</b>	<b>24</b>
<b>3.2.4. Loading and measurement .....</b>	<b>25</b>
<b>3.3. Experiment results .....</b>	<b>27</b>
<b>3.3.1. Crack simulation by EAFP.....</b>	<b>27</b>
<b>3.3.2. Results of pull-out test.....</b>	<b>30</b>
<b>3.3.2.1. Failure mode .....</b>	<b>30</b>
<b>3.3.2.2. Pull-out load and slip.....</b>	<b>31</b>
<b>3.4. Bond strength degradation.....</b>	<b>33</b>

3.4.1. Comparison of the results with the fib model code 2010 .....	33
3.4.2. Bond degradation and surface crack width relationship .....	35
3.5. Conclusions .....	37
<b>Chapter 4 Bond Degradation of Rebars in Cracked Concrete due to Rebar corrosion: Side-Splitting Case.....</b>	<b>38</b>
4.1. Introduction.....	38
4.2. Experiment outline.....	38
4.2.1. Pull-out specimen and materials.....	38
4.2.1. Crack simulation by EAFP.....	41
4.2.2. Loading and measurement .....	42
4.3. Experiment results .....	44
4.3.1. Crack simulation by EAFP.....	44
4.3.1. Results of pull-out test.....	46
4.3.1.1. Failure mode .....	46
4.3.1.1. Pull-out load and slip.....	49
4.3.1.2. Crack opening versus slip .....	52
4.4. Bond strength degradation.....	53
4.4.1. Comparison of the results with the fib model code 2010 and JCI 1998 .....	53
4.4.1. Bond degradation and surface crack width relationship .....	54
4.5. Conclusions.....	56
<b>Chapter 5 Conclusions .....</b>	<b>57</b>
<b>DEDICACES .....</b>	<b>58</b>
<b>REFERENCES .....</b>	<b>59</b>

## *List of Figures*

Fig. 1.1 Mechanical interaction between concrete and deformed steel bar .....	6
Fig. 1.2 Sequences and consequences of corrosion on reinforcements[2] .....	7
Fig. 1.3 Case of single-splitting.....	9
Fig. 1.4 Case of side-splitting.....	9
Fig. 1.5 Schematic illustration of the methodology followed in the present study .....	10
Fig. 2.1 Concrete cracking with expansion agent.....	12
Fig. 2.2 Specimen for cracking confirmation.....	13
Fig. 2.3 Crack width over time.....	13
Fig. 2.4 Scheme of aluminum pipe with rib .....	14
Fig. 2.5 Picture of aluminum pipe with rib .....	14
Fig. 2.6 Position of strain gauges.....	15
Fig. 2.7 Loading setup .....	16
Fig. 2.8 Strain and time relationship after filling the expansion agent .....	17
Fig. 2.9 Failure of the specimen .....	19
Fig. 2.10 Stress-strain relationship .....	20
Fig. 3.1 Aluminum pipe with ribs .....	22
Fig. 3.2 Specimen detail .....	23
Fig. 3.3 Picture of the mold.....	23
Fig. 3.4 Filling of expansion agent .....	24
Fig. 3.5 Loading and measurement setup .....	25
Fig. 3.6 Teflon sheet.....	26
Fig. 3.7 Picture of specimen at loading.....	26
Fig. 3.8 Cracking of concrete after filling the expansion agent.....	28
Fig. 3.9 Distribution of crack width.....	29
Fig. 3.10 Splitting with crack opening and newly generated crack .....	30
Fig. 3.11 Splitting with crack opening only.....	30
Fig. 3.12 Load-slippage relationship.....	32
Fig. 3.13 Maximum pull-out load vs crack width.....	33
Fig. 3.14 Result in comparison with fib Model Code 2010 .....	34
Fig. 3.15 Result and prediction model .....	35
Fig. 4.1 Specimen details.....	39
Fig. 4.2 Specimen mold .....	39
Fig. 4.3 Filling of the expansion agent .....	41
Fig. 4.4 Loading and measurement setup .....	42
Fig. 4.5 Picture of specimen at loading.....	43
Fig. 4.6 Teflon sheet.....	43
Fig. 4.7 Cracking of concrete after filling the expansion agent.....	44
Fig. 4.8 Distribution of crack width.....	45
Fig. 4.9 Failure mode.....	47
Fig. 4.10 Damage inside the bond part .....	48
Fig. 4.11 Pull-out load versus slip at free-end for 18 MPa specimens .....	50
Fig. 4.12 Pull-out load versus slip at free-end for 30 MPa specimens .....	51
Fig. 4.13 Maximum pull-out load versus crack width before loading.....	52
Fig. 4.14 Crack opening versus slip .....	52
Fig. 4.15 Comparison with fib model 2010 and JCI 1998.....	53
Fig. 4.16 Result and prediction model .....	54
Fig. 4.17 Proposed evaluation formula from test result.....	55

### *List of Tables*

<b>Table 2.1 Dimension of aluminum pipe with rib .....</b>	<b>14</b>
<b>Table 2.2 List of specimens.....</b>	<b>14</b>
<b>Table 2.3 Strain before loading.....</b>	<b>16</b>
<b>Table 2.4 Tensile test results.....</b>	<b>19</b>
<b>Table 3.1 Concrete proportion of used concrete .....</b>	<b>23</b>
<b>Table 3.2 Concrete mechanical properties.....</b>	<b>24</b>
<b>Table 3.3 Specimen list.....</b>	<b>24</b>
<b>Table 3.4 Crack level.....</b>	<b>29</b>
<b>Table 3.5 Maximum crack width .....</b>	<b>29</b>
<b>Table 3.6 Test result list.....</b>	<b>31</b>
<b>Table 3.7 fib model code 2010 .....</b>	<b>34</b>
<b>Table 3.8 Regression analysis result .....</b>	<b>35</b>
<b>Table 3.9 Comparison of the calculated and experimental values .....</b>	<b>36</b>
<b>Table 4.1 Specimen list.....</b>	<b>40</b>
<b>Table 4.2 Concrete mix proportion .....</b>	<b>40</b>
<b>Table 4.3 Concrete mechanical properties.....</b>	<b>40</b>
<b>Table 4.4 Mechanical properties of reinforcement .....</b>	<b>40</b>
<b>Table 4.5 Maximum crack width .....</b>	<b>46</b>
<b>Table 4.6 Test result list.....</b>	<b>48</b>
<b>Table 4.7 Regression analysis result .....</b>	<b>54</b>

# Chapter 1 Introduction

## 1.1. Background

To guarantee the composite action of reinforced concrete members, the bond at the steel-concrete interface is an important property of reinforced concrete. It allows the forces to be transferred from the reinforcement to the surrounding concrete in a structure. The scientists who have contributed to the knowledge of the many aspects of bonding agree that the bond stress includes three components: chemical adhesion, friction, and mechanical interlock (see Fig. 1.1) [1]. When the rebar is in tension, the concrete crushing and splitting occur due to mainly the mechanical interlock. It is considered that the bond between reinforcement and concrete has a large influence on the structural behavior of RC members. Therefore, to get satisfactory performance of RC structures, it is necessary to assure adequate bond.

However, the deterioration of RC structures due to the corrosion of rebar is now becoming a demanding problem.

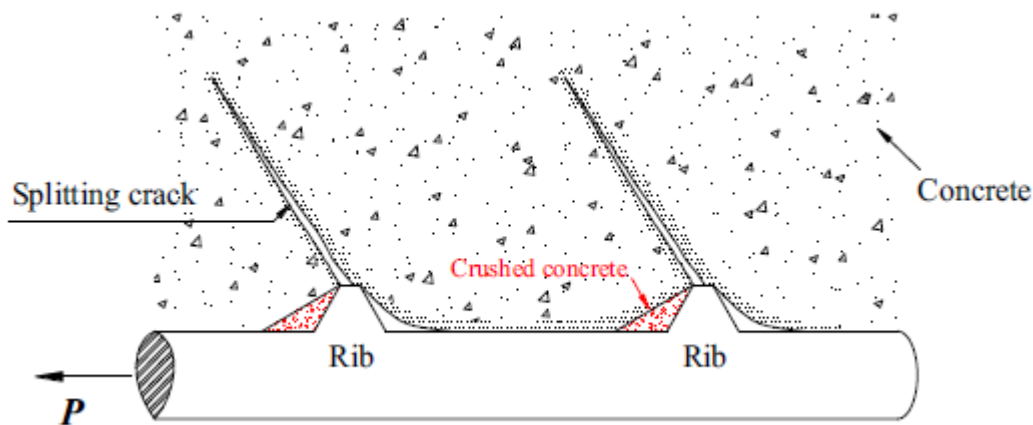


**Fig. 1.1 Mechanical interaction between concrete and deformed steel bar**

In recent decades, lots of RC structures are threatened by corrosion worldwide, causing huge direct and indirect costs annually. As shown in Fig. 1.2 [2], bond deterioration can negatively affect the structural properties of RC structures. This was confirmed in many studies. To better estimate the mechanical properties of corroded RC structures through theoretical analysis or numerical modeling, it is essential to fully understand how corrosion affects bond.

Many studies investigated the degradation of bond strength due to the corrosion of reinforcement which causes cracks along bars. Relevant bond tests were carried out by many researchers, these studies have developed numerical models which are in good agreement with test results [3] [4] [5].

However, even if these current models can give a good prediction, there are still some limitations when they are put into practice. One of the most significant current discussions is that these models mostly use the steel section loss or mass loss as a variable, which is very difficult to measure in existing structures that are under services conditions. Regarding the corrosion of rebars in reinforced concrete, the surface crack width provides the clearest visual manifestation. It is a key parameter to solve this problem by directly correlating the bond deterioration of the surface crack width because it can be easily measured. A rough correlation between bond strength reduction and surface crack width is proposed in the fib Model Code 2010 [6]. On another hand, most studies use accelerated electrical corrosion techniques. The combination of the effect of cracking and the formation of rust around the bar can lead to difficulties in analyzing the processes at a fundamental level. Also, when concrete cracks

without corrosion, those results could be difficult to use.

Very little is currently known about the potential correlations between the bond and the surface crack width. However, further investigations with this respect should be performed to give more experimental evidence.

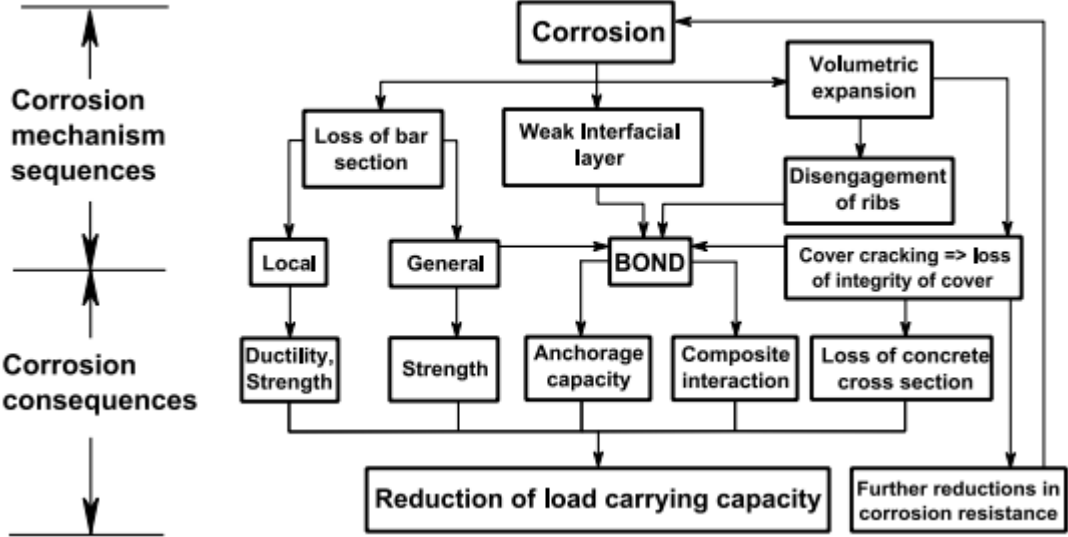


Fig. 1.2 Sequences and consequences of corrosion on reinforcements[2]

## **1.2. Objectives of this study**

The major aim of this study is to increase the knowledge of the bond behavior in reinforced concrete structures with cracks due to corrosion, as well as investigating the possible links between visual inspection data (crack width) and bond degradation. To achieve this goal, there are some specific objectives which relate to the different stages of the research project:

- Testing the tensile properties of ribbed aluminum pipe filled with an expansion agent
- Investigating the bond degradation with different crack width along the reinforcing bars.
- Investigating the bond behavior with different crack width occurring on the surrounding concrete

## **1.3. Methodology of this study**

The scientific approach of this study has been primarily based on experiments and corresponding observations. The simulation of the cracking of concrete due to corrosion of reinforcing bars by using an aluminum pipe embedded in concrete and filled with an expansion agent was used as a novel method to simulate reinforcing bars in which volume expands due to corrosion. Throughout this thesis, the abbreviation ‘EAFP’ is used to refer to the expansion agent filled pipe. With the increase of the crack width over elapsed time from filling of expansion agent, a target crack width can easily be obtained.

First, for grasping the mechanical properties of EAFP, tensile tests of the aluminum pipes with ribs are carried out. In addition, two series of experiments are carried out to study the effect of induced crack width on bond degradation. The one end pull-out test is conducted with a short bond length designed to enable the focus on local bond behavior. The splitting cracks plays a fundamental role of reducing the bond, therefore two cases are set: “Single-split type” when the induced cracks are along the rebar (Fig. 1.3) and “Side split-type” when the induced cracks are located on the surroundings of concrete (Fig. 1.4). The simulated cracks on specimens are measured before the tests. During the test, the pull-out load, slippage at the free end of the rebar and the opening of the width of the induced crack are measured. These data are compared to those in the existing literature. Regression analysis is also conducted to propose a simple model for evaluating the bond degradation with crack width as the main variable. Fig. 1.5 shows a schematic illustration of the methodology followed in this study.

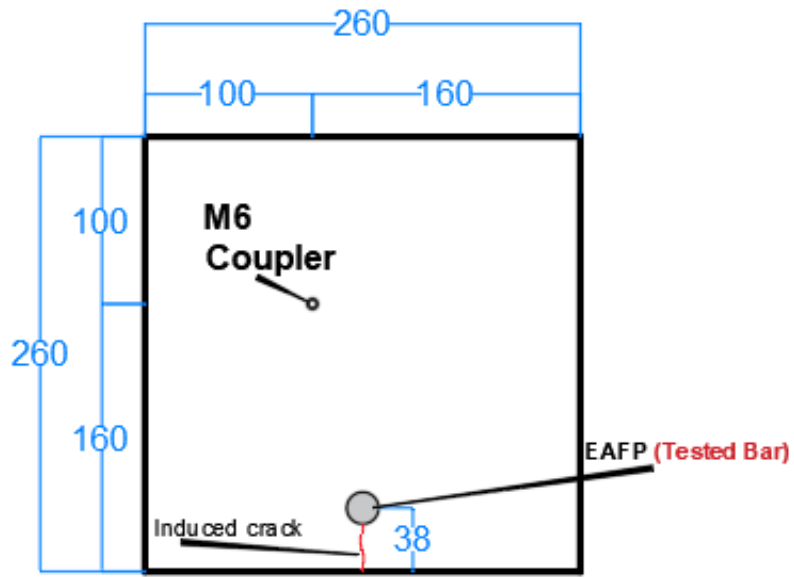


Fig. 1.3 Case of single-splitting

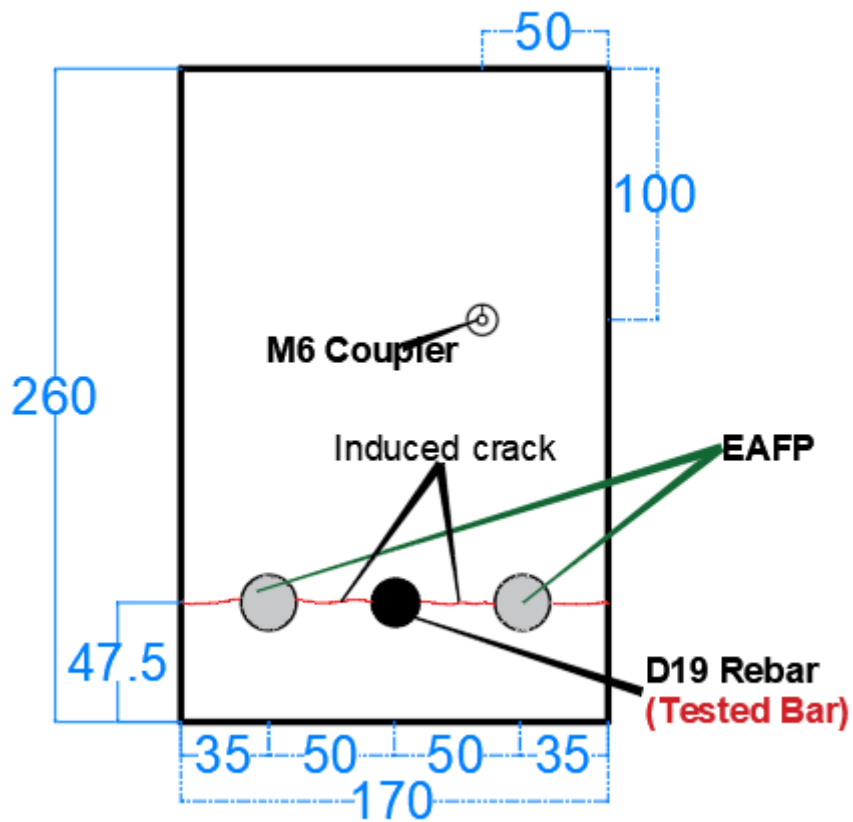
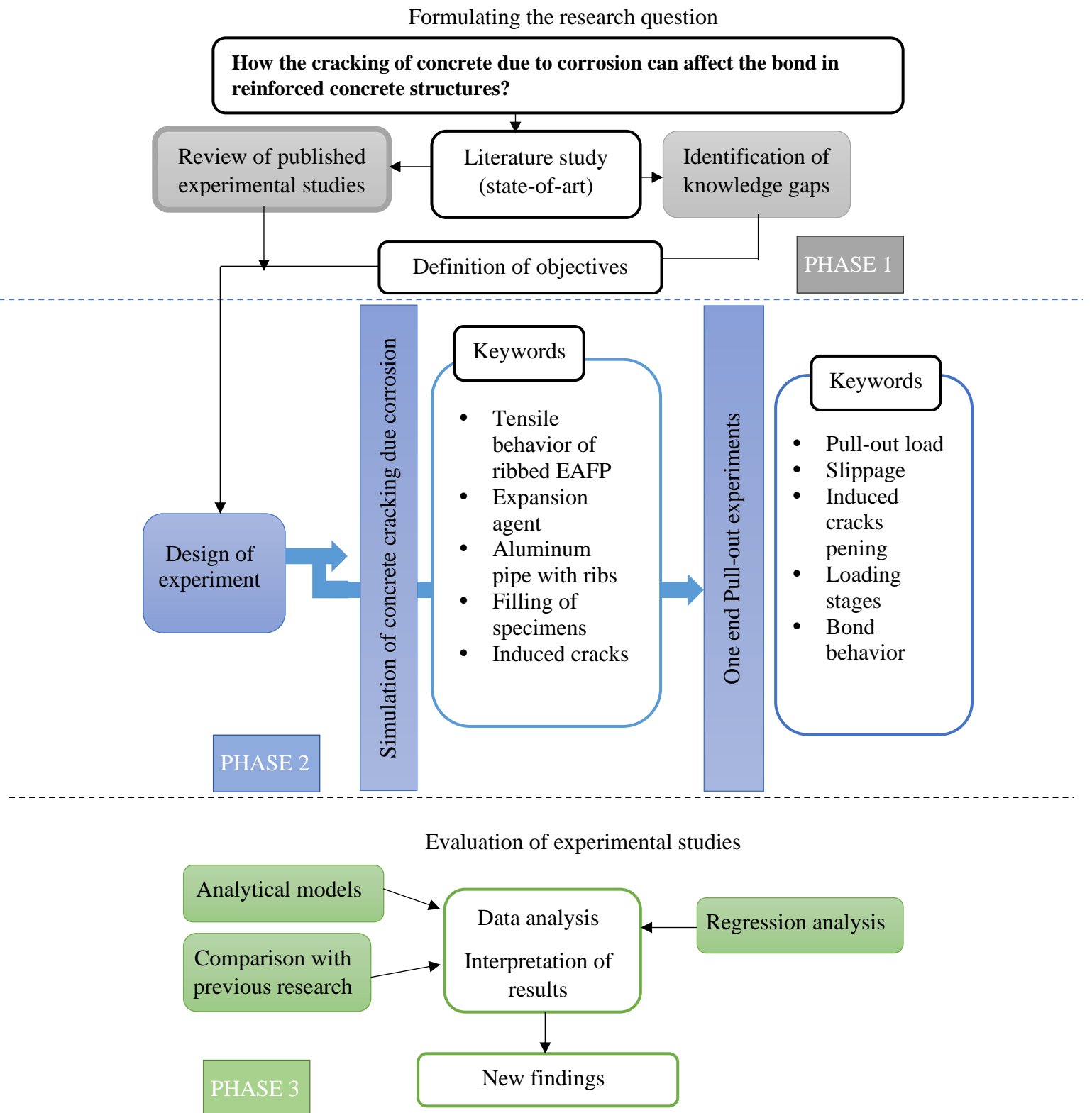


Fig. 1.4 Case of side-splitting



**Fig. 1.5 Schematic illustration of the methodology followed in the present study**

#### **1.4. Outline of the thesis**

The thesis consists of 5 chapters. In Chapter 1, the background, objectives, and methodology of the study are provided. In order to grasp the mechanical properties of ribbed aluminum pipes filled with an expansion agent when the pipe replaces reinforcing bars, the tensile tests of those pipes are carried out, therefore Chapter 2 presents the tensile properties of ribbed aluminum pipe filled with an expansion agent. Chapter 3 present the pull-out study of the Single-split specimen when the splitting cracks are parallel or along the rebar. Chapter 4 outlines the pull-out experience in case of “Side split”, in other words when the splitting cracks are perpendicular to the rebar. Conclusions and suggestions for future research are placed in Chapter 5.

## Chapter 2 Tensile properties of ribbed aluminum pipe filled with an expansion agent

### 2.1. Introduction

The possibility to simulate the cracking of concrete due to corrosion of reinforcing bars in the laboratory in a relatively short time by using EAFP was demonstrated. In this chapter, in order to grasp the mechanical properties of EAFP when the pipe replaces reinforcing bars, tensile tests of those pipes are carried out.

### 2.2. Background of crack simulation by aluminum pipe filled with an expansion agent

Many studies have been conducted about the effects of reinforcing bar corrosion on the structural performance of RC members using experiments that simulate cracks due to corrosion expansion of reinforcing bars by an electrolytic corrosion test or by slits in the previous research, but the conformity to real cracks is unclear. At the Kanakubo lab, in the University of Tsukuba, an aluminum pipe embedded in concrete and filled with an expansion agent has been proposed as a method to simulate reinforcing bars whose volume expands due to corrosion.

An expansion agent is mainly used for the destruction of rocks and RC structures. In powder form, it expands when humidified. Due to this expansion, cracks are generated in the concrete (see Fig. 2.1).

Fig.2.2 shows the specimen used in order to confirm the possibility of crack simulation [7]. An aluminum pipe with 18 mm as outer diameter and 1 mm thickness was embedded in the concrete. The compressive strength of the concrete was 25.3 MPa and the ratio of the water to expansion agent was 30%. The specimen was placed as the axial direction of the pipe was set vertically, and an expansion agent was filled from the top of the pipe

As can be seen in Fig.2.3, the possibility to simulate the cracking of concrete due to corrosion of reinforcing bars in the laboratory in a relatively short time was confirm. Also, it was found that the crack width can be easily targeted due to the fact that cracks width increases over time.

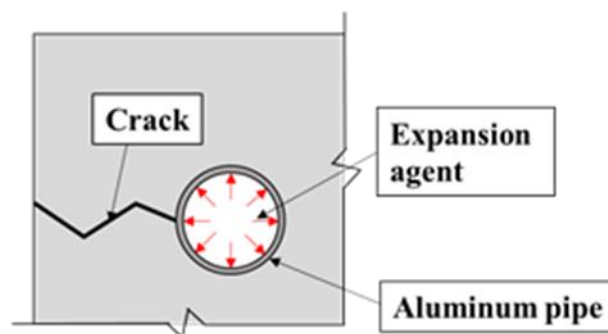
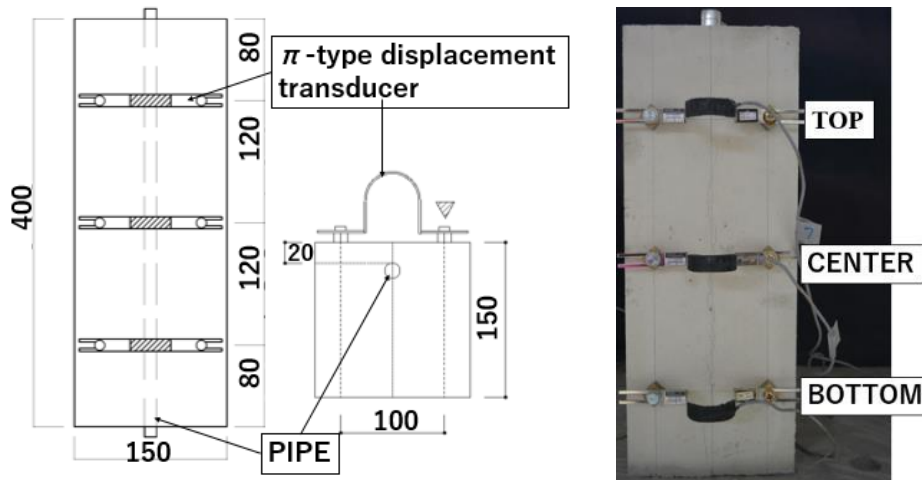
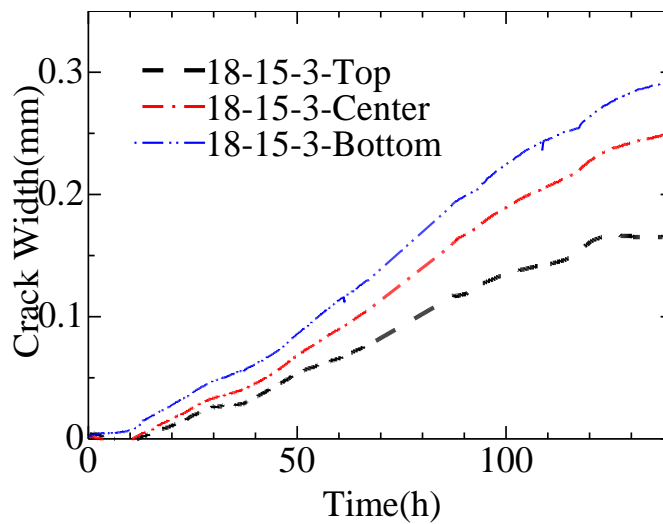


Fig. 2.1 Concrete cracking with expansion agent



**Fig. 2.2 Specimen for cracking confirmation**



**Fig. 2.3 Crack width over time**

### 2.3. Experiment outline

#### 2.3.1. Specimen Overview

According to JIS G 3112 (Steel bars for concrete reinforcement), the ribs were machined on an aluminum pipe. In order to simulate a deformed bar D19 with an aluminum pipe with an outer diameter of 21.7mm and a thickness of 2.5mm was used. The details of the aluminum pipe with ribs are shown in Fig.2.4 and Table 2.1. Table 2.2 summarizes the list of specimens. The test was conducted on specimen filled with an expansion agent or not. For specimens without expansion agent, three with ribs and three without ribs were set. 5 specimens with ribs were filled with an expansion agent and a target strain before loading was taken as the main parameter.

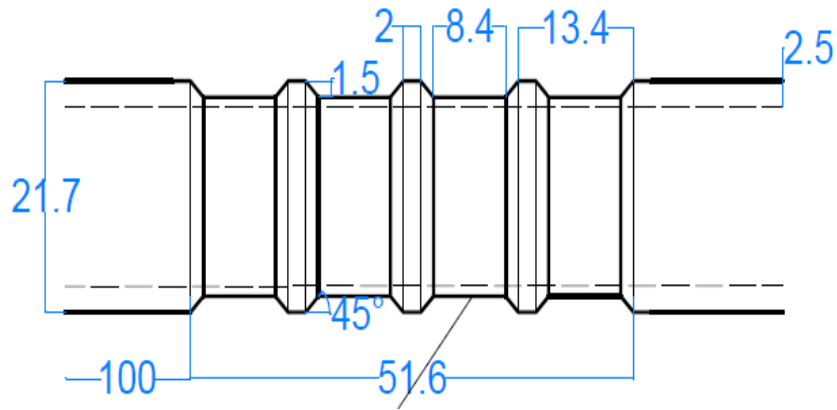


**Fig. 2.4 Scheme of aluminum pipe with rib**



**Fig. 2.5 Picture of aluminum pipe with rib**

**Table 2.1 Dimension of aluminum pipe with rib**

Pipe diameter( $d$ ) (mm)	Height of ribs ( $h$ ) (mm)	Interval between ribs( $l$ ) (mm)	$h/l$	$h/d$	$l/d$
21.70	1.50	13.40	0.11	0.07	0.61

**Table 2.2 List of specimens**

Specimen	Ribs	Expansion Agent	Target strain before loading	Number of specimens
P19-NRNF	No	No	—	3
P19-RNF	Yes		—	3
P19-RF1		Yes	0.3%	1
P19-RF2			0.5%	1
P19-RF3			0.8%	1
P19-RF4			1.0%	1
P19-RF5			1.2%	1

### 2.3.2. Loading and Measurement

As shown in Fig.2.6, strain gauges were fixed, and the time course of axial strain after expansion agent filling and circumferential strain on and between ribs were measured. The variable factor was the target axial strain at the start of the tensile test, with a range of 0.3% to 1.2%.

Monotonic tensile loading was carried out using a universal testing machine of 500 kN capacity. Fig.2.7 shows the loading and measurement method for tension tests. To prevent the deformation of the grasped part by the chuck, round steel bars having a length of 80 mm were inserted into the specimen ends. In addition to the load, the axial and circumferential strain were measured.

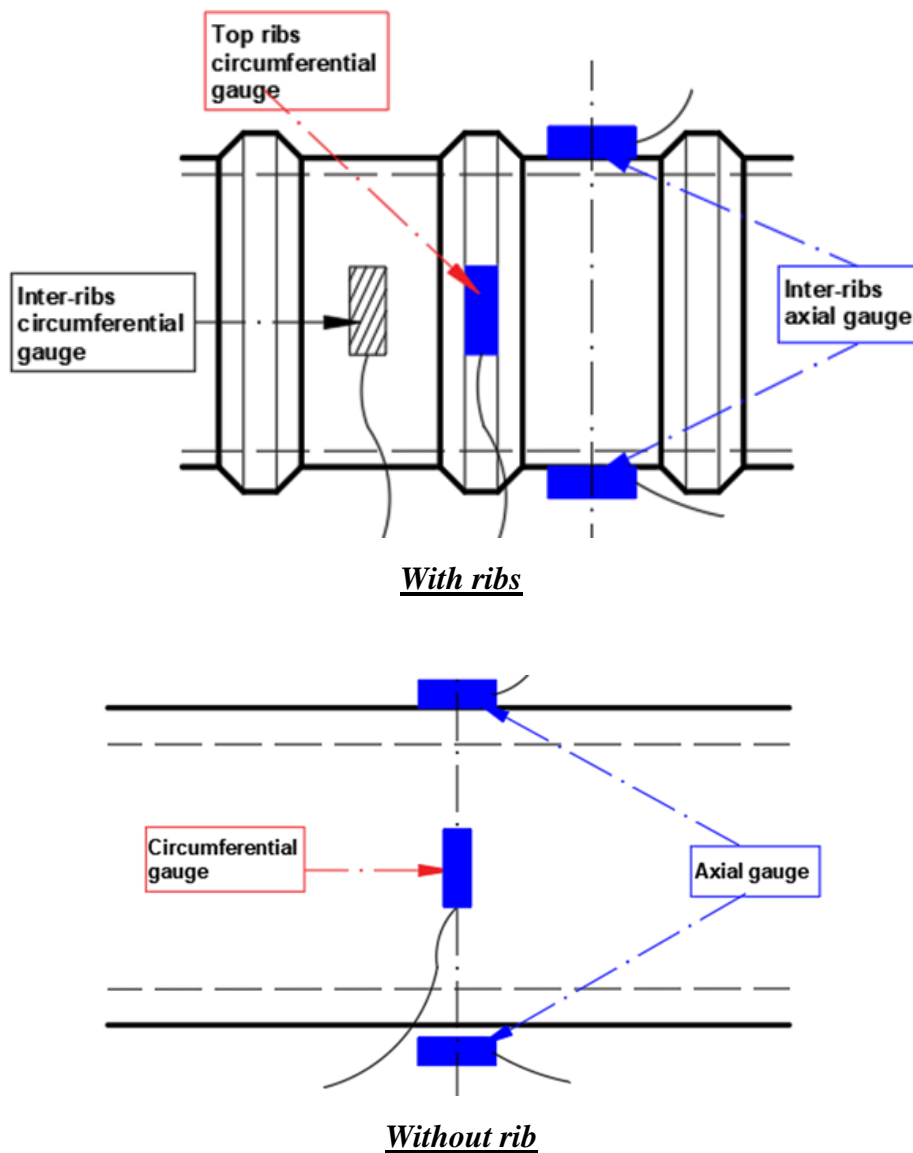
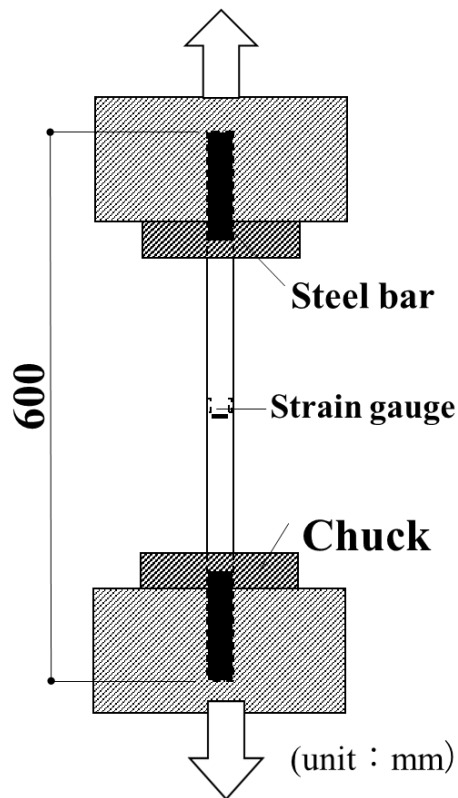


Fig. 2.6 Position of strain gauges



**Fig. 2.7 Loading setup**

## 2.4. Experiment results

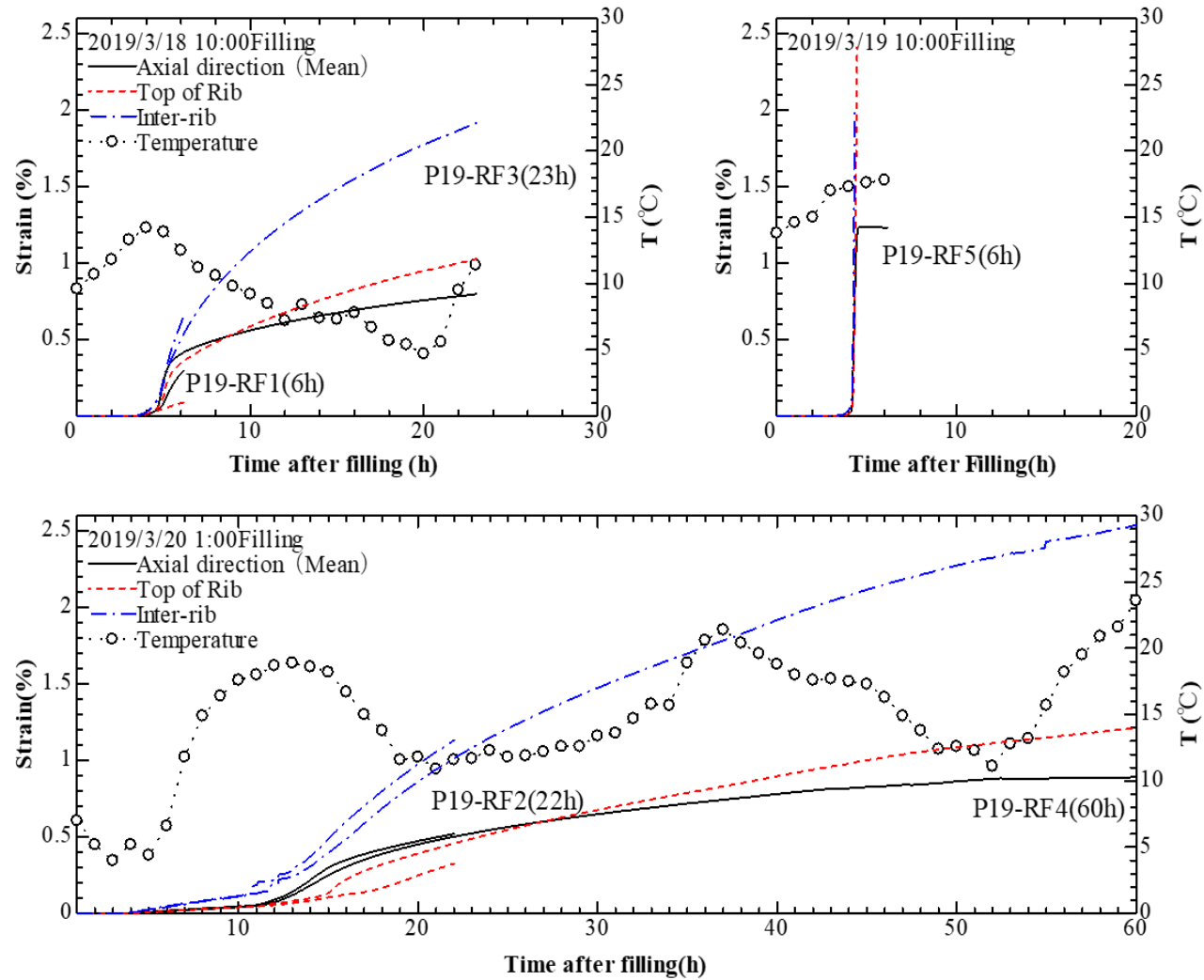
### 2.4.1. Strain before loading due to the expansion agent

Table 2.3 summarizes the strain due to the effect of the expansion agent before the loading. For the specimen P19-RF5, due to the peeling of gauge during measurement after filling the expansion agent, the circumferential strain was not measured. Fig.2.8 shows the progression of each strain after filling the expansion agent. The temperatures in the figure were obtained from the Japan Meteorological Agency located in Tsukuba city. The axial strain and circumferential strain increased both over time, and the inter-rib circumferential strain was larger. The speed of the reaction sharply increases between 4 to 10 hours after filling the expansion agent and tends to slow down. 4 hours after filling the expansion agent, the strain evolution is greatly affected by the temperature. This phenomenon is remarkably observed when the temperature exceeded 15 ° C.

**Table 2.3 Strain before loading**

Specimen	Axial strain (%)	Circumferential strain on top of the rib (%)	Inter-ribs Circumferential strain (%)
P19-RF1	0.297	0.088	0.664
P19-RF2	0.521	0.328	1.13
P19-RF3	0.799	1.04	1.93
P19-RF4	0.892	1.21	2.54
P19-RF5	1.23	—*	—*

\* Due to the peeling of gauge during measurement after filling the expansion agent, these strains were not measured.



**Fig. 2.8 Strain and time relationship after filling the expansion agent**

#### 2.4.2. Tensile test results

The tensile test results are shown in Table 2.4. Fig.2.9 shows examples of the fracture of the specimen after loading.

The tensile stress was calculated dividing the load by the cross-sectional area of the aluminum pipe. For the specimen without ribs, the cross-section is 150.8 mm<sup>2</sup> and 55.6 mm<sup>2</sup> for one with ribs.

Fig.2.10 shows the stress-strain relationship of the loaded specimen. The yield strength of specimens without expansion agent (P19-NRNF and P19-RN) was taken when the stress becomes almost constant just after the elastic region. The yield strength of the other test specimens was obtained by 0.2% offset strength from the axial strain.

The modulus of elasticity was calculated by the least-squares method in a section that can be regarded as the elastic zone in the stress-strain curve. Similarly, the absolute value of Poisson's ratio was calculated using the inter-ribs strain. It was obtained by dividing the elastic modulus by the lateral elastic modulus. Two gauges points were marked at the specimen before loading. The percentage of elongation after failure was determined by dividing the deformation distance by the initial distance before loading.

According to the result, there is no evidence that the presence of ribs and the filling of an expansion agent has an influence on the tensile strength. For all specimens, the tensile strength is from 210 to 220 MPa.

On another hand, for the specimen without an expansion agent, no significant differences in yield strength and elastic modulus are found between the specimens with ribs and ones without ribs.

At the beginning of the loading, with the increasing of the axial strain, the yield strength and modulus of elasticity of the pipe filled with an expansion agent increase too. However, the elongation at failure tended to decrease. The tensile strength was not affected.

It can be seen that the presence of the ribs tends to decrease the Poisson's ratio. A possible explanation for this might be that the occurrence of restraint in the circumferential direction at the ribs decreases the transversal elastic modulus between ribs.

**Table 2.4 Tensile test results**

Specimen	Max load (kN)	Tensile strength (MPa)	Yield strength (MPa)	Young modulus (GPa)	Poisson's ratio (%)	Elongation (%)
P19-NRNF	33.02	219	96.7	74.4	0.341	—
P19-RNF	12.00	216	102	78.2	0.247	8.5
P19-RF1	11.78	212	97.5	64.0	0.239	7.6
P19-RF2	11.67	210	121	63.6	0.226	7.0
P19-RF3	11.56	208	146	84.0	—	5.9
P19-RF4	11.84	213	158	70.2	0.162	5.3
P19-RF5	12.34	222	170	95.7	—	3.9



**Fig. 2.9 Failure of the specimen**

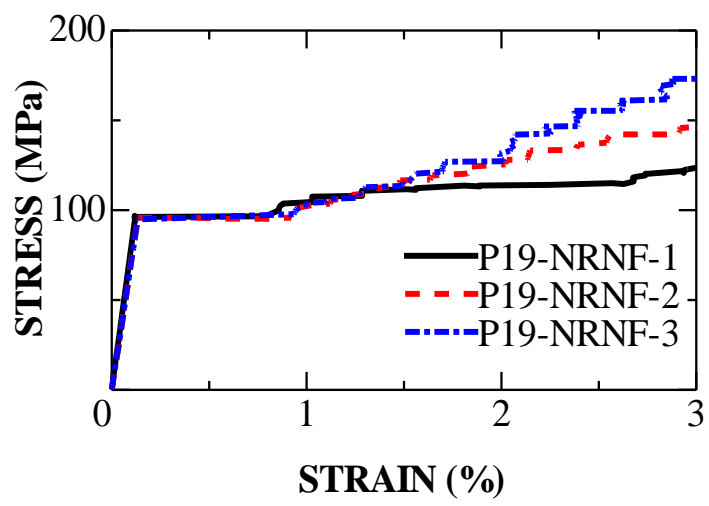
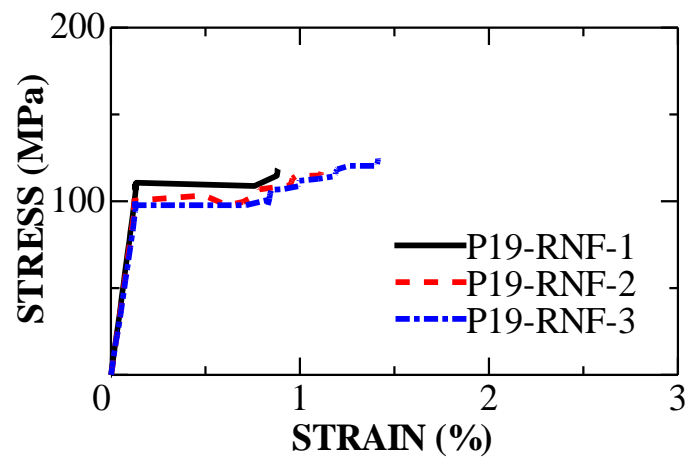
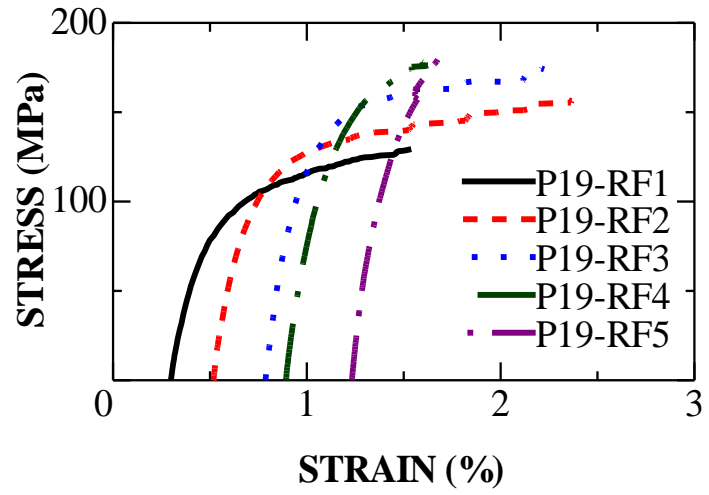


**Fig. 2.10 Stress-strain relationship**

## **2.5. Conclusions**

The aim of this chapter was to examine the mechanical properties of ribbed aluminum pipes filled with an expansion agent when the pipe replaces reinforcing bars. The experiment confirmed that:

- The strain in the axis, top and between the ribs tended to increase over the time after the filling of the expansion agent.
- There is no evidence that the presence of ribs and the filling of an expansion agent has an influence on the tensile strength.
- The presence of the ribs tends to decrease the Poisson's ratio
- At the beginning of the loading, with the increasing of the axial strain, the yield strength and modulus of elasticity of the pipe filled with an expansion agent increase too. However, the elongation at failure tended to decrease. The tensile strength is not affected.

# Chapter 3 Bond Degradation of Rebars in Cracked Concrete due to Rebar Corrosion: Single Splitting Case

## 3.1. Introduction

In this chapter, to develop a simple formula for the bond strength of a corroded bar with surface crack width as a variable, the pull-out test is conducted on a concrete block with an embedded bar following different corrosion crack width simulated by EAFP. The test is carried out on a single split type specimen as described previously. One advantage of using this simulation method is that it allows focussing on the effect of the cracking while ignoring the section loss.

A rough correlation between bond strength reduction and surface crack width is suggested by the fib Model Code 2010. In addition to that Japan Concrete Institute in the concrete structure rehabilitation research committee report 1998 gave an evaluation formula of the bond degradation as a function of corrosion, also an overview of the current research indicates that existing studies have achieved a primary knowledge regarding the potential correlation between bond and the surface crack width. However, there still a research gap in this respect.

## 3.2. Experiment outline

### 3.2.1. Aluminum pipe with ribs

Fig. 3.1 shows an overview of a processed aluminum pipe with ribs set according to JIS G 3112. An aluminum pipe with 21.7 mm as outer diameter and 2.5mm thickness was used to imitate the D19 rebar. The fundamental properties of the aluminum pipe and the expansion agent filled pipe have been reported in Chapter 2.

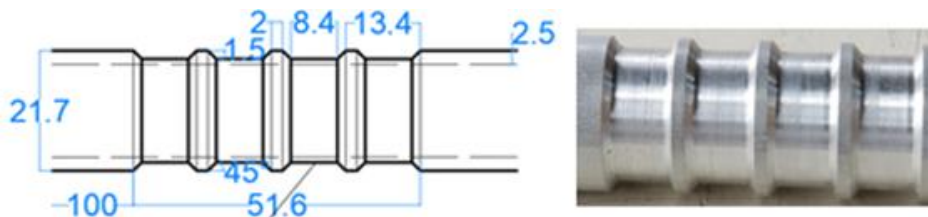


Fig. 3.1 Aluminum pipe with ribs

### 3.2.2. Pull-out specimen

The pull-out specimen was designed as shown in Fig.3.2. The dimensions of the specimen were 260×260×82mm and the aluminum pipe with ribs was embedded at 38mm from the specimen side. The framework is shown in Fig. 3.3. The bond length of 51.6mm was chosen to avoid the rupture of the pipe by tensile force. Moreover, an unbonded part was set to avoid cone failure of concrete. The M6 coupler was fixed 100×100 mm at the up left position to set a LDVT for measuring the slip of pipe. A  $\pi$ -type displacement transducer was placed on the concrete cover to measure the opening of crack during loading. Table 3.1 shows the mix proportion of used concrete and Table 3.2 shows the mechanical properties of concrete obtained from the concrete cylinder test on the day of filling of expansion agent. Table 3.3 shows the list of specimens. The test variable was set on the level of crack width induced by expansion agent

filled pipe before pullout loading. A total of 12 specimens were tested.

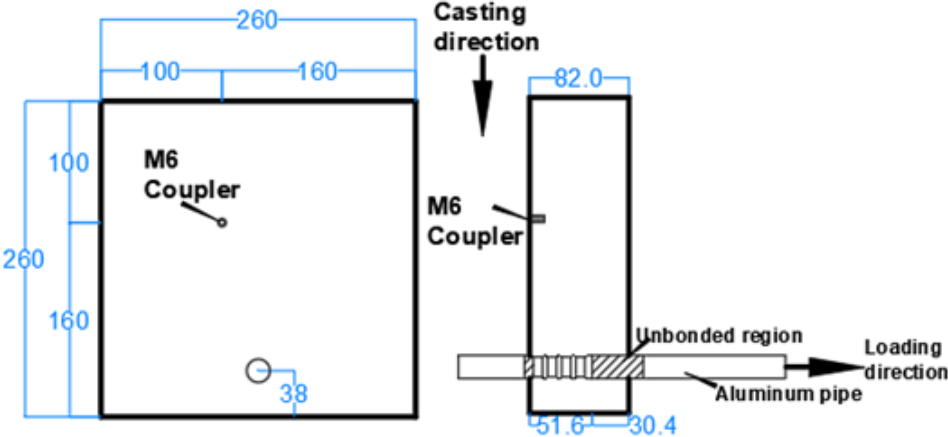


Fig. 3.2 Specimen detail



Fig. 3.3 Picture of the mold

Table 3.1 Concrete proportion of used concrete

Water-cement ratio (%) W/C	Cement (kg/m <sup>3</sup> )	Water (kg/m <sup>3</sup> )	Air	Fine Aggregate (kg/m <sup>3</sup> )	Coarse Aggregate (kg/m <sup>3</sup> )	Water Reducing Agent (kg/m <sup>3</sup> )
82.5	242	200	4.5 %	937	827	2.42

**Table 3.2 Concrete mechanical properties**

Compressive strength (MPa)	Young's modulus (GPa)	Splitting tensile strength (MPa)
17.8	22.8	1.78

**Table 3.3 Specimen list**

Specimen name	Cover Thickness	Expected crack level	Number of specimens
S-L1	38mm	Level 1	12
S-L2		Level 2	
S-L3		Level3	

**3.2.3. Crack simulation by EAFP**

The ratio of the water to an expansion agent was set to 30%. The specimen was placed as the axial direction of the pipe was set vertically, and an expansion agent was filled from the top of the pipe as shown in Fig.3.4. With the increase of the crack width over elapsed time after filling of expansion agent, a target crack width was easily obtained by using the time after filling as a parameter.



**Fig. 3.4 Filling of expansion agent**

### 3.2.4. Loading and measurement

The loading was carried out at Kanakubo lab in the University of Tsukuba. Fig. 3.5 shows the general set-up for the pull-out test. The specimen was placed on the Teflon sheet and the loading plate on which the hole with the same diameter corresponding to concrete cover in order to not restrict the lateral deformation of concrete. This detail can be seen from Fig 3.6 and Fig.3.7 The pipe was subjected to monotonic pull-out loading at a speed of 0.5mm/min with a Universal Testing Machine. The measurement items are pull-out load, crack opening and slippage of the pipe at the free end.

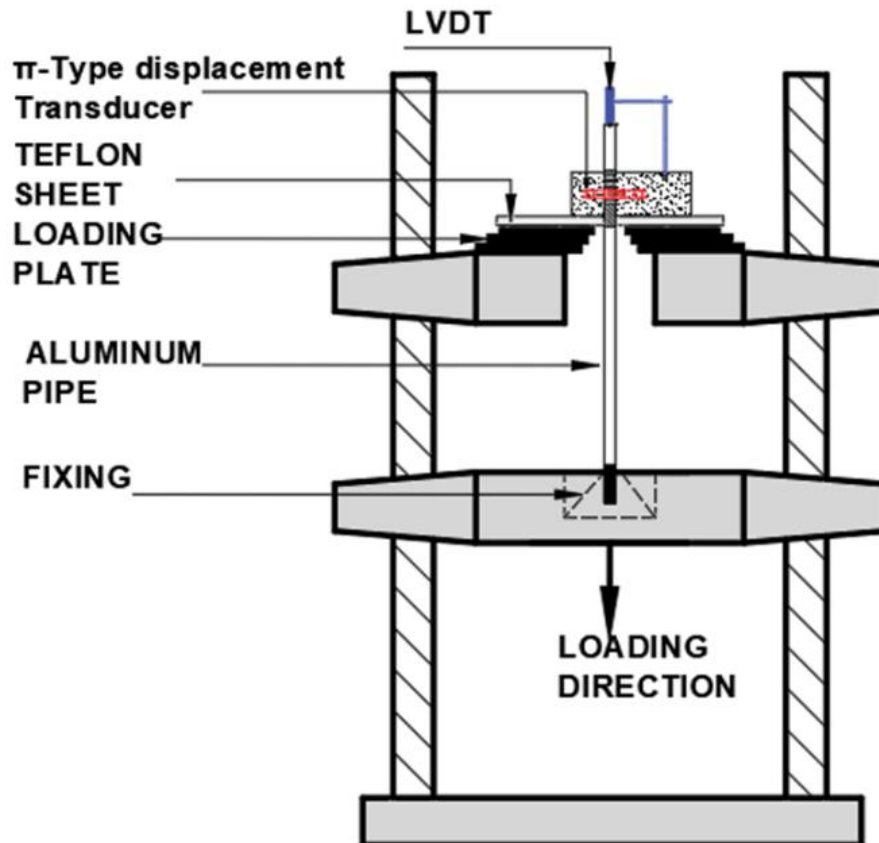


Fig. 3.5 Loading and measurement setup



**Fig. 3.6 Teflon sheet**



**Fig. 3.7 Picture of specimen at loading**

### **3.3. Experiment results**

#### **3.3.1. Crack simulation by EAFP**

Fig. 3.8 shows an example of crack patterns after filling the expansion agent. The expansion agent reaction was heavily influenced by the ambient temperature, so to control the width of the crack, specimens were placed in variable temperature conditions. Also, because cracks continued to grow after filling the expansion agent, crack width was measured only when growth had stopped fully.

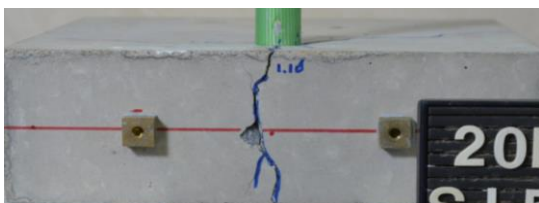
Cracks were categorized according to their width, as shown in Table 3.4. The maximum crack width in every specimen is summarized in Table 3.5. To better observe the distribution of cracking among the specimens, the maximum cracks widths are plotted in Fig 3.9.



(a) Top view



(b) Bottom view



(c) Side view

**Fig. 3.8 Cracking of concrete after filling the expansion agent**

**Table 3.4 Crack level**

Level	Crack width range
Level 1	$\leq 0.5\text{mm}$
Level 2	0.5mm to 1.0mm
Level 3	$> 1.0\text{mm}$

**Table 3.5 Maximum crack width**

Specimen name	Maximum crack width (mm)
S-1-L1	0.15
S-2-L1	0.1
S-3-L1	0.2
S-4-L1	0.35
S-2-L2	0.5
S-1-L2	1.0
S-1-L3	1.5
S-2-L3	3.0
S-3-L3	2.0
S-4-L3	1.8
S-5-L3	2.0
S-6-L3	2.6

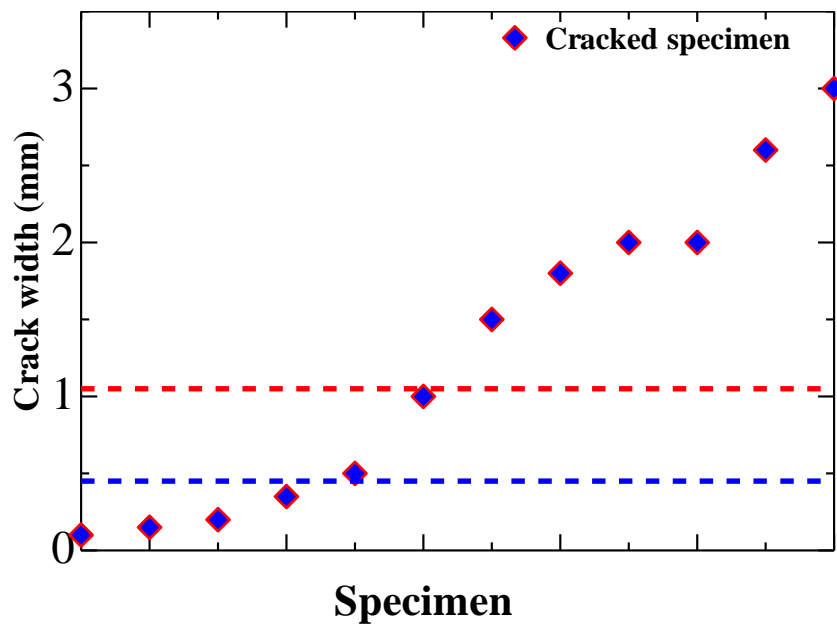
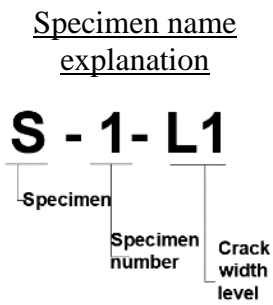


**Fig. 3.9 Distribution of crack width**

### 3.3.2. Results of pull-out test

#### 3.3.2.1. Failure mode

All specimens experienced failure due to splitting. A group of specimens failed by newly generated splitting crack despite existing longitudinal crack due to corrosion as shown in Fig.3.10 and other specimens failed by widening of existing crack induced by the expansion agent as can be seen in Fig.3.11. The results of pull-out tests are summarized in Table 3.6.

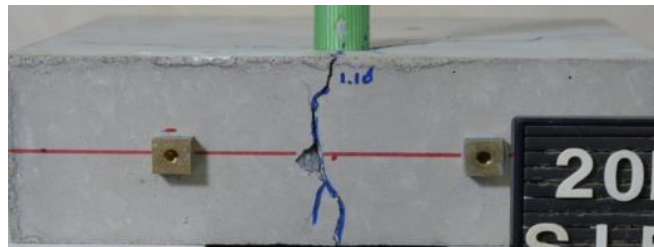


*Before loading*

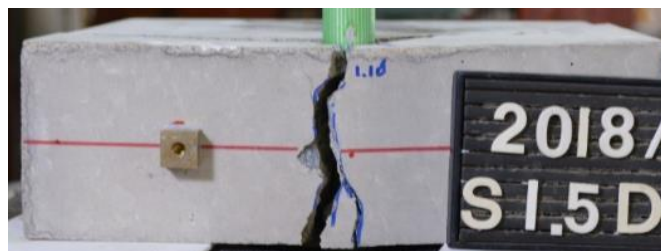


*After loading*

**Fig. 3.10 Splitting with crack opening and newly generated crack**



*Before loading*



*After loading*

**Fig. 3.11 Splitting with crack opening only**

**Table 3.6 Test result list**

Specimen name	Biggest crack width (mm)	At Maximum		Remarks
		Load (kN)	Slippage (mm)	
S-1-L1	0.15	7.99	0.088	New crack
S-2-L1	0.1	8.39	0.146	Crack opening
S-3-L1	0.2	6.96	0.218	New crack
S-4-L1	0.35	5.79	0.144	New crack
S-2-L2	0.5	6.14	0.198	New crack
S-1-L2	1.0	6.99	0.890	New crack
S-1-L3	1.5	4.11	0.262	Crack opening
S-2-L3	3.0	2.12	0.804	Crack opening
S-3-L3	2.0	3.77	0.572	Crack opening
S-4-L3	1.8	4.69	0.658	Crack opening
S-5-L3	2.0	3.92	0.768	Crack opening
S-6-L3	2.6	2.30	1.380	Crack opening

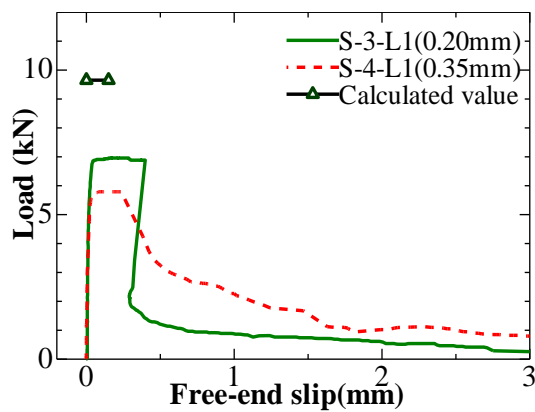
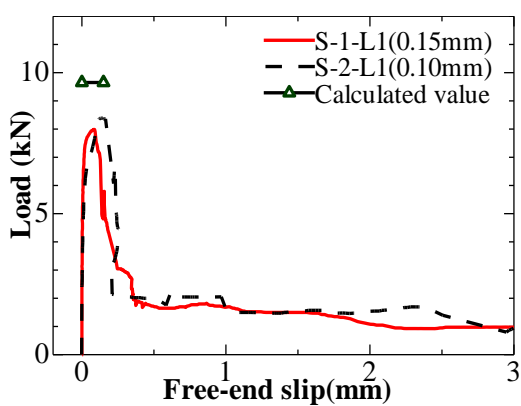
### 3.3.2.2. Pull-out load and slip

The pull-out load versus slippage relationships are shown in Fig. 3.12. In the case of Level 3 cracks, the load – slippage relationship tends not to results in a severe decrease of load after maximum pull out force. The maximum pull-out load versus crack width relationship is shown in Fig. 3.13. It can be seen that the maximum load decreases as the crack width increases. As expected, there is a significant correlation between residual bond strength and induced crack width.

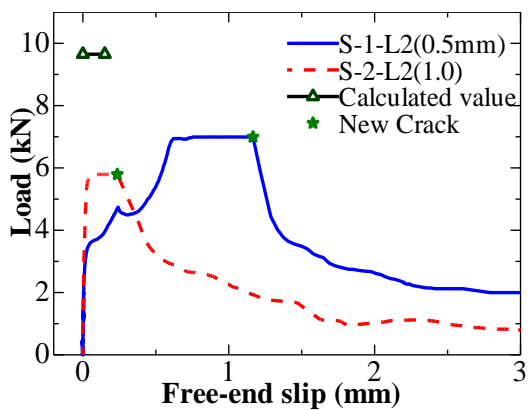
To better observe the degradation due to the induced crack, the maximum pull-out load is normalized by calculated pull-out splitting strength as reported in the previous study [8] as a non-cracked specimen using the following equation:

$$\tau_{b,max} = 0.601 \cdot \sigma_t \cdot (r_u/d_b) \cdot \cot \alpha$$

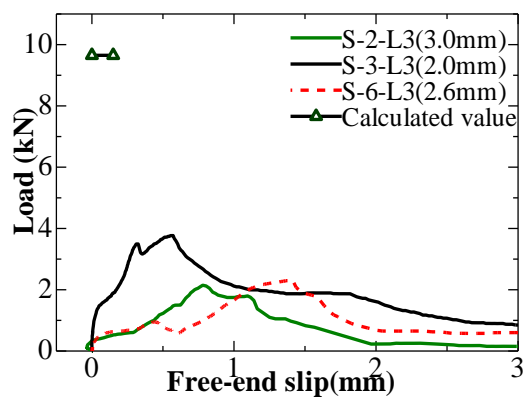
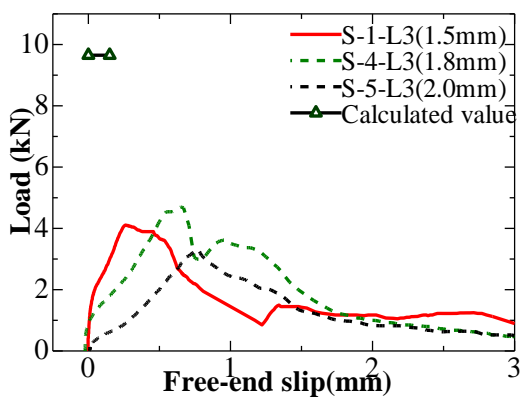
where,  $\tau_{b,max}$  : bond splitting strength,  $\sigma_t$ : splitting tensile strength of concrete,  $r_u: C+d_b/2$ ,  $d_b$ : diameter of the pipe (19mm),  $C$ : the thickness of cover concrete,  $\alpha$ : the angle between the longitudinal axis and splitting force (=34 degree).



*Level 1*



*Level 2*



*Level 3*

**Fig. 3.12 Load-slippage relationship**

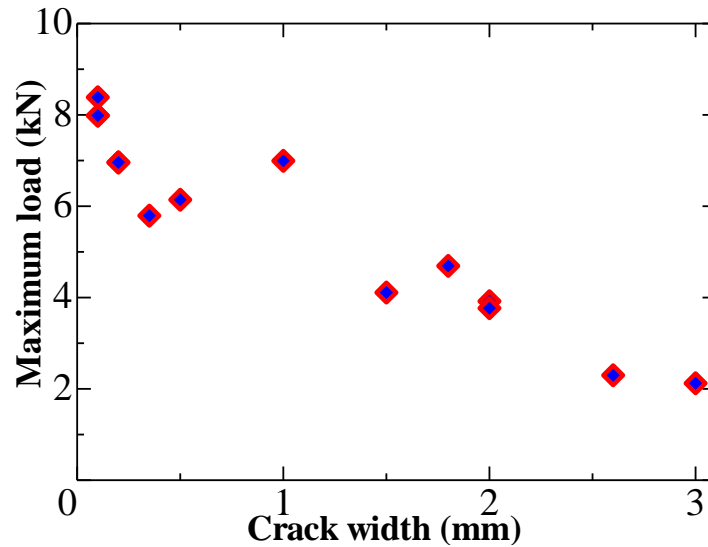


**Fig. 3.13 Maximum pull-out load vs crack width**

### **3.4. Bond strength degradation**

#### **3.4.1. Comparison of the results with the fib model code 2010**

In the fib Model Code 2010[6], the reduction in bond strength depending on the surface crack width was introduced. For a certain range of surface crack width, the possible variation of the pull-out load degradation can be predicted as shown in Table 3.7. The first development of cracks at corrosion penetrations (i.e. reductions in rebar radius) of between 0.015mm and 0.040mm was reported. Also, a relationship between crack width and corrosion penetration as corrosion progressed was derived.

In this study, the proposed relationship is compared with the test results in Fig. 3.14. The prediction with Model Code 2010 is in good agreement with Level 1 (crack width  $\leq 0.5$ mm) and for the specimen with 2.6mm and 3mm as crack width as an extrapolation. However, for Level 2 (crack width 0.5mm to 1.0mm), the fib Model Code 2010 gives underestimation. It should be noted that the authors of the fib model code 2010 assume that the residual strength of concrete structures is also affected by cross-section loss of steel. In this study, only on the influence of the induced crack in the concrete cover is focused on. Only the bond degradation of level 2 specimens was higher than the prediction from the fib Model Code. This finding was unexpected and suggests that when the crack width is between 0.5mm to 1 mm, the influence of the bar profile change becomes greater. Interestingly, Yang et al (2019) [9] found that corrosion crack in concrete is concluded to be a more dominant factor than the corroded rebar shape and rust accumulation in bond deterioration mechanism.

**Table 3.7 fib model code 2010**

Corrosion penetration (mm)	Equivalent surface crack (mm)	Confinement	Residual capacity %	
			Ribbed	Plain
0.05	0.2-0.4	No links	50-70	70-90
0.1	0.4-0.8		40-50	50-60
0.25	1.0-2.0		25-40	30-40
0.05	0.2-0.4	Links	95-100	95-100
0.10	0.4-0.8		70-80	95-100
0.25	1.0-2.0		60-75	90-10

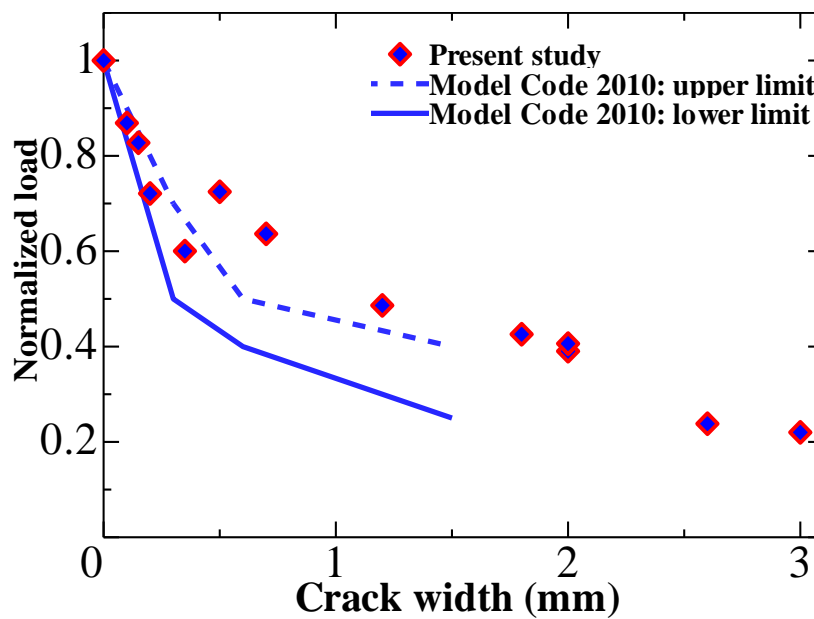


**Fig. 3.14 Result in comparison with fib Model Code 2010**

### 3.4.2. Bond degradation and surface crack width relationship

As mentioned in the literature review, the existing models related to bond deterioration focus on the relationship between bond strength and mass loss, and they are mostly formulated as linear, exponential or logarithmic equations. The present study proposes a simple formula for the bond strength of corroded bar with surface crack width as a variable and thus contributes to accurately assess the effects of deterioration.

As can be seen from the results of regression analysis in Table 3.8, an exponential equation provides the best fit (higher R<sup>2</sup>). Therefore, the following equation can be used for the prediction of the maximum pull-out load:

$$P_{(W_{cr})} = P_0 \cdot e^{-0.515W_{cr}}$$

where  $P_{(W_{cr})}$ : Pull-out strength in cracked concrete;  $P_0$ : Pull-out strength of specimen without crack;  $W_{cr}$ : Crack width.

Fig 3.15 shows the experimental result and the prediction formula comparison. The calculated and experimental results are compared in Table 3.9. The ratios of the experimental to calculated values are close to one, which indicates that the concrete crack width can potentially be a good indicator to characterize bond strength degradation.

**Table 3.8 Regression analysis result**

Analysis	Equations	R <sup>2</sup>
<i>Linear</i>	$-0.306W_{cr}+1$	0.66
<i>Logarithmic</i>	$0.175\ln(W_{cr}) + 0.4916$	0.80
<i>Exponential</i>	$e^{-0.515 W_{cr}}$	0.91

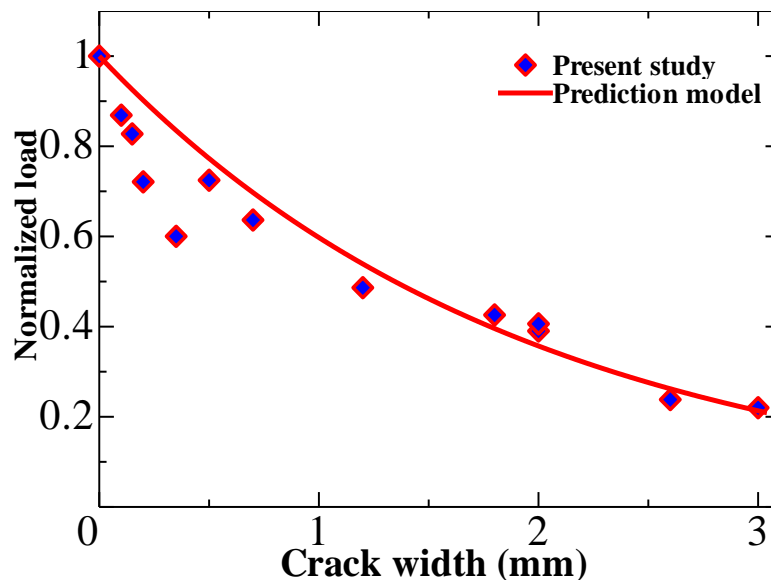


**Fig. 3.15 Result and prediction model**

**Table 3.9 Comparison of the calculated and experimental values**

Specimen name	Biggest crack width (mm)	Experimental maximum load (kN)	Calculated maximum load (kN)	Exp /Cal
S-1-L1	0.15	7.99	8.93	0.89
S-2-L1	0.1	8.39	9.16	0.91
S-3-L1	0.2	6.96	8.70	0.80
S-4-L1	0.35	5.80	8.06	0.72
S-2-L2	0.5	6.14	6.72	0.91
S-1-L2	1.0	6.99	7.46	0.94
S-1-L3	1.5	4.11	3.81	1.07
S-2-L3	3.0	2.12	2.05	1.03
S-3-L3	2.0	3.77	3.44	1.09
S-4-L3	1.8	4.69	5.20	0.90
S-5-L3	2.0	3.92	3.44	1.13
S-6-L3	2.6	2.30	2.52	0.90

### **3.5. Conclusions**

In this chapter, the pull-out test is conducted on 12 concrete blocks with an embedded bar following different corrosion crack widths simulated by EAFP. The test is carried out on a single split type.

The prediction with Model Code 2010 is in good agreement with Level 1 (crack width  $\leq 0.5\text{mm}$ ) and for the specimen with 2.6mm and 3mm as crack width as an extrapolation.

There was a significant exponential correlation between pull-out strength and surface crack width. Also, a simple formula to predict bond degradation is proposed by using the surface crack width as the main variable.

# Chapter 4 Bond Degradation of Rebars in Cracked Concrete due to Rebar Corrosion: Side-Splitting Case

## 4.1. Introduction

In this chapter, a concrete cracked by EAFP in bond test specimens has been designed to fail with side splitting of the cover. Those specimens are subjected to a pull-out test and a relationship between the maximum pull-out load of bar and surface crack width as a variable is discussed.

## 4.2. Experiment outline

### 4.2.1. Pull-out specimen and materials

The pull-out specimen was designed as shown in Fig.4.1. The dimensions of the specimen were 260×170×170mm and the D19 rebar is embedded at 47.5mm ( $2.5d_b$ ) from the specimen cover side. The framework is shown in Fig. 4.2. A short bond length of 4 times the diameter of the rebar equal to 76 mm was chosen to focus on the local bond. To simulate the cracking of the surrounding concrete of the rebar, 2 aluminum pipes with a diameter of 22mm and a thickness of 1mm were set to 50mm from the rebar. Moreover, an unbonded part was set to avoid cone failure of concrete. The M6 coupler was fixed 100×50 mm at the upright position to set a LDVT for measuring the slip of the free end of the bar. Two  $\pi$ -type displacement transducers were placed on the top and two others on the east and west side of the specimen to measure the opening of crack during loading. Table 4.1 shows the list of the specimens. Table 4.2 shows the mix proportion of used concrete and Table 4.3 shows the mechanical properties of concrete obtained from the concrete cylinder test on the day of filling of expansion agent. The reinforcement is a deformed bar of a nominal diameter of 19 mm. Its mechanical properties are presented in Table 4.4.

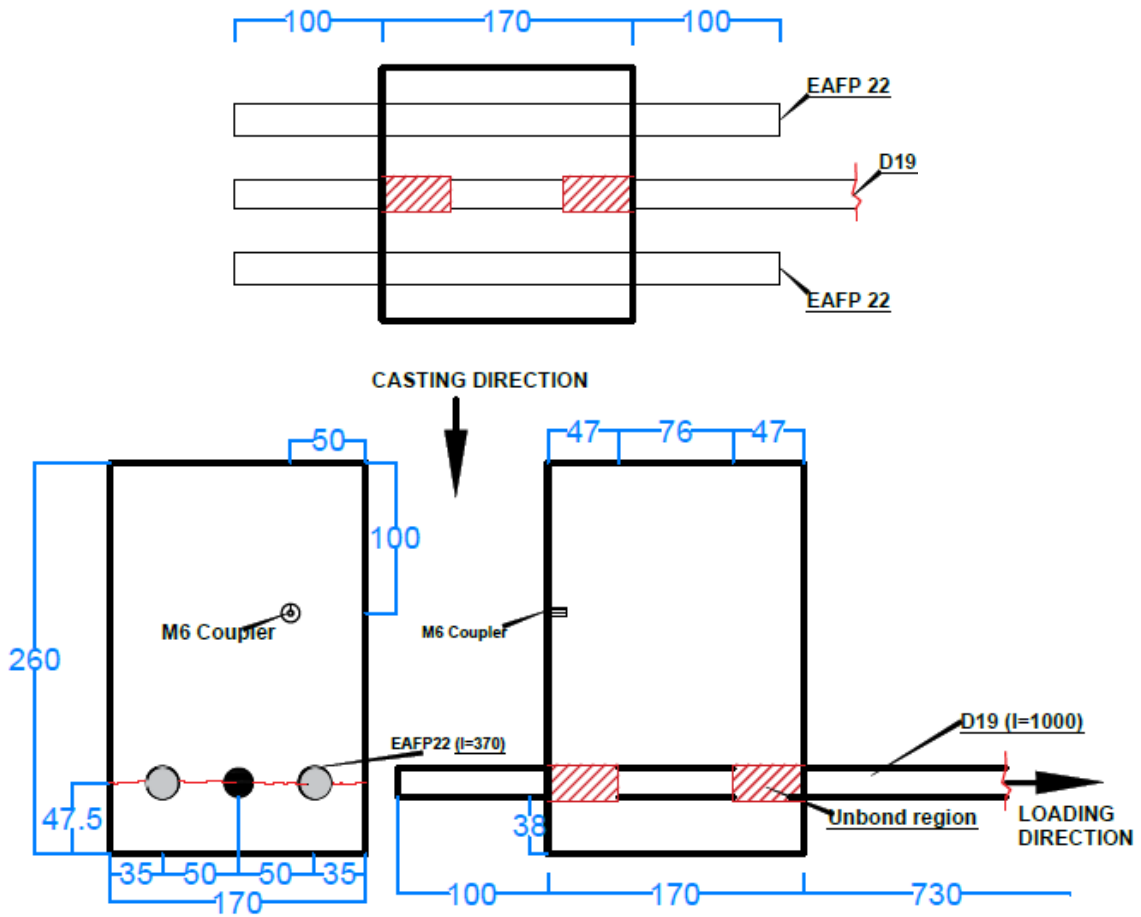


**Fig. 4.1 Specimen details**

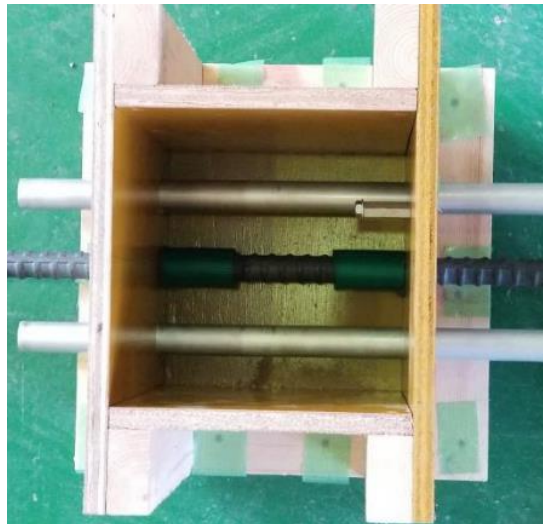


**Fig. 4.2 Specimen mold**

**Table 4.1 Specimen list**

Series	Specimen name	Concrete target strength	Induced crack	Number of specimens
I	S.18.NC	18MPa	No	2
	S.18.C.		Level 1 - 3	6
II	S.30.NC	30MPa	No	2
	S.30. C		Level 1 - 3	6

**Table 4.2 Concrete mix proportion**

Concrete target strength	W/C (%)	Unit weight (kg/m <sup>3</sup> )				
		<i>C</i>	<i>W</i>	<i>S</i>	<i>G</i>	<i>Ad</i>
18MPa	78.5	245	192	942	852	2.45
30MPa	56.0	321	180	846	918	3.21

**Table 4.3 Concrete mechanical properties**

Concrete target strength	Compressive strength (MPa)	Young modulus (GPa)	Splitting strength (MPa)
18MPa	21.8	19.0	2.26
30MPa	31.7	21.6	2.59

**Table 4.4 Mechanical properties of reinforcement**

Nominal diameter	Tensile strength (MPa)	Yield strength (MPa)	Young modulus (GPa)
19	535	366	193

#### 4.2.1. Crack simulation by EAFP

The ratio of the water to the expansion agent was set to 30%. The specimen was placed as the axial direction of the pipes was set vertically, and an expansion agent was filled from the top of the pipes as shown in Fig.4 .3.



Fig. 4.3 Filling of the expansion agent

#### 4.2.2. Loading and measurement

The loading was carried out at Kanakubo lab in the University of Tsukuba. Fig. 4.4 shows the general set-up for the pull-out test. The specimen was placed on the Teflon sheet and the loading plate on which the hole with the same diameter corresponding to concrete cover in order to not restrict the lateral deformation of concrete. This detail can be seen from Fig 4.5 and Fig.4.6. The D19 rebar was subjected to monotonic pull-out loading at a speed of 0.5mm/min with a Universal Testing Machine. The measurement items are pull-out load, crack opening and slippage of the D19 rebar at the free end.

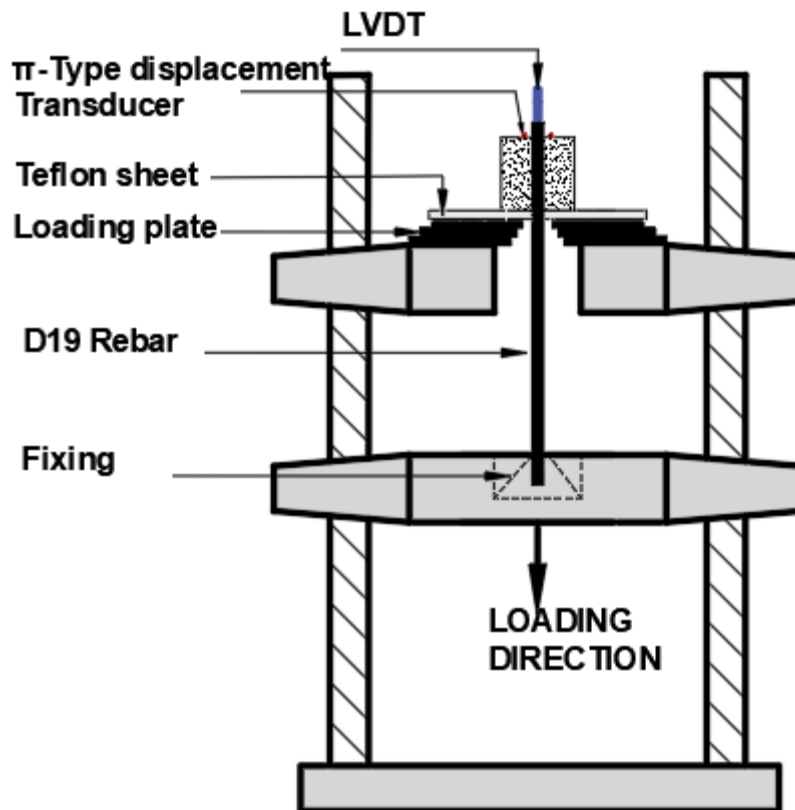
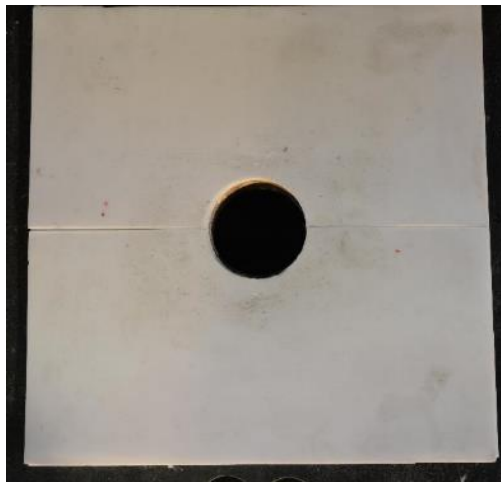


Fig. 4.4 Loading and measurement setup



**Fig. 4.5** Picture of specimen at loading



**Fig. 4.6** Teflon sheet

### 4.3. Experiment results

#### 4.3.1. Crack simulation by EAFP

Fig. 4.7 shows an example of crack patterns after filling the expansion agent. The expansion agent reaction was heavily influenced by the ambient temperature, so to control the width of the crack, specimens were placed in variable temperature conditions. Also, because cracks continued to grow after filling the expansion agent, crack width was measured only when the target crack width was attained.

The maximum crack width on the top side (bottom side at the filling) in every specimen is summarized in Table 4.5. To better observe the distribution of cracking among the specimens, the maximum cracks widths was are plotted in Fig 4.8.



Fig. 4.7 Cracking of concrete after filling the expansion agent

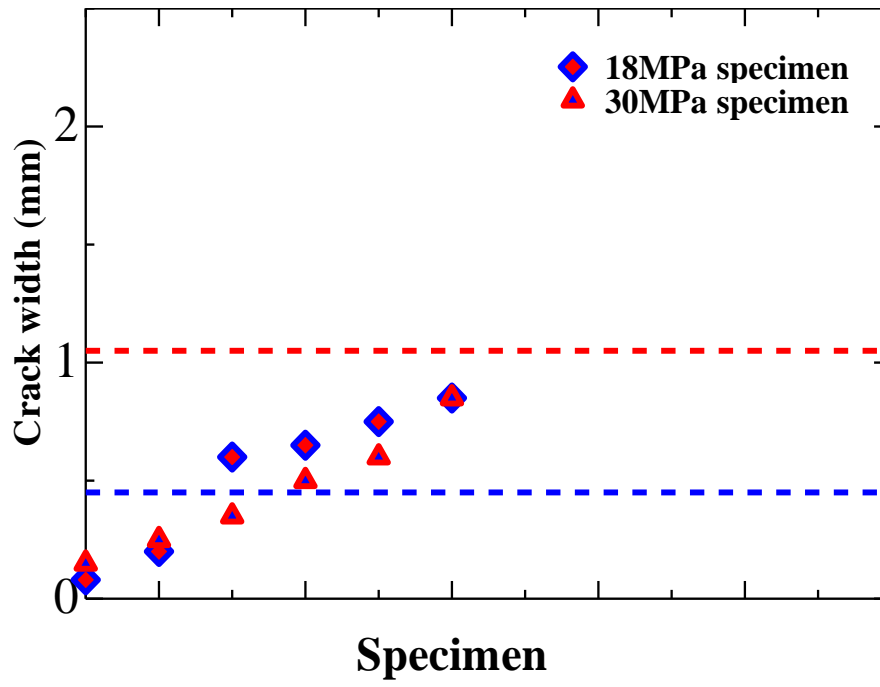


Fig. 4.8 Distribution of crack width

**Table 4.5 Maximum crack width**

Specimen name	Crack width (mm)		
	Top side	East side	West side
S.18.NC.1	0	0	0
S.18.NC.2	0	0	0
S.18.C.0.08	0.08	0.40	0.40
S.18.C.0.2	0.20	0.40	0.40
S.18.C.0.6	0.60	1.20	1.20
S.18.C.0.65	0.65	1.00	1.20
S.18.C.0.75	0.75	1.30	1.20
S.18.C.0.85	0.85	1.00	1.00
S.30.NC.1	0	0	0
S.30.NC.2	0	0	0
S.30.C.0.15	0.15	0.35	0.35
S.30.C.0.25	0.25	0.80	0.70
S.30.C.0.35	0.35	0.80	0.85
S.30.C.0.50	0.50	1.00	1.00
S.30.C.0.60	0.60	1.30	1.20
S.30.C.0.85	0.85	1.40	1.30

#### **4.3.1. Results of pull-out test**

##### **4.3.1.1. Failure mode**

All specimens experienced failure due to splitting. The specimens without crack failed by single splitting due to the limited cover thickness. In the crack induced specimens, most of them failed by side-splitting due to the opening of pre-existent cracks. In side-splitting failure, some specimens presented newly side crack (named N1 with one new crack, named N2 with two new cracks). All the failure modes are summarized in Fig 4.9. Depending on the failure mode, concrete between the ribs was totally damaged or without any damage. This can be seen in Fig 4.10. The results of pull-out tests are shown in Table 4.6.



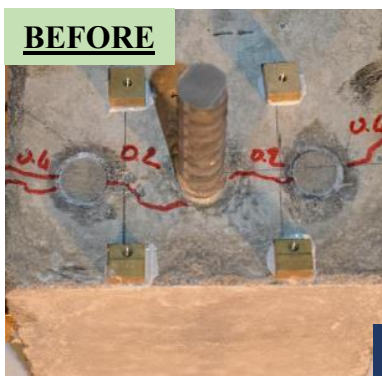
SINGLE SPLITTING



SIDE SPLITTING



SIDE SPLITTING N1



SIDE SPLITTING N2



Fig. 4.9 Failure mode



**Fig. 4.10 Damage inside the bond part**

**Table 4.6 Test result list**

Specimen name	Crack width (mm)	At Maximum load		Remarks
		Load (kN)	Slip (mm)	
S.18.NC.1	0	50.51	0.444	Single split
S.18.NC.2	0	46.36	0.962	Single split
S.18.C.0.08	0.08	31.36	0.508	Side split N1
S.18.C.0.2	0.20	22.87	0.352	Side split N2
S.18.C.0.6	0.60	17.22	0.832	Side split O
S.18.C.0.65	0.65	25.10	0.121	Side split N1
S.18.C.0.75	0.75	4.19	1.102	Side split O
S.18.C.0.85	0.85	4.29	0.676	Side split O
S.30.NC.1	0	42.97	0.592	Single split
S.30.NC.2	0	61.73	0.166	Single split
S.30.C.0.15	0.15	49.46	0.348	Single split
S.30.C.0.25	0.25	31.25	0.308	Single split
S.30.C.0.35	0.35	26.86	0.468	Side split O
S.30.C.0.50	0.50	33.20	0.61	Side split O
S.30.C.0.60	0.60	19.77	0.488	Side split N1
S.30.C.0.85	0.85	12.53	0.724	Side split O

#### **4.3.1.1. Pull-out load and slip**

During the pull-out tests, the slippage of the D19 rebar is measured so the pull-out load versus the slip relationship can be plotted in Fig. 4.11 for 18 MPa and in Fig.4.12 for 30MPa. A plot of the pull-out load – slippage relationship of a typical uncracked and cracked specimen shows that the slope of the initial ascending branch seems to not change with the present number, indicating a no decrease in stiffness. As the pull-out load increase, the slip seems to increase in an almost linear way. As soon as the bond strength is reached however, a steeper descending curve is measured for uncracked specimens when compared to cracked ones. Hence a more sudden bond degradation is noted due to the occurrence of new cracks or the opening of the induced cracks.

The maximum pull-out load versus crack width before loading relationship is shown in Fig. 4.13. It can be seen that the maximum load decreases as the crack width increases. As expected, there is a significant correlation between residual bond strength and induced crack width.

The decrease of the pull-out load is more severe in 18MPa specimens than in 30 MPa specimens. A possible explanation for this might be that the 30MPa concrete has a stiffer response than the 18MPa concrete in both compression and tension therefore the crack opening may be delayed. Another possible explanation for this is that the confinement effect developed by the same concrete cover is perhaps more effective in 30MPa concrete.

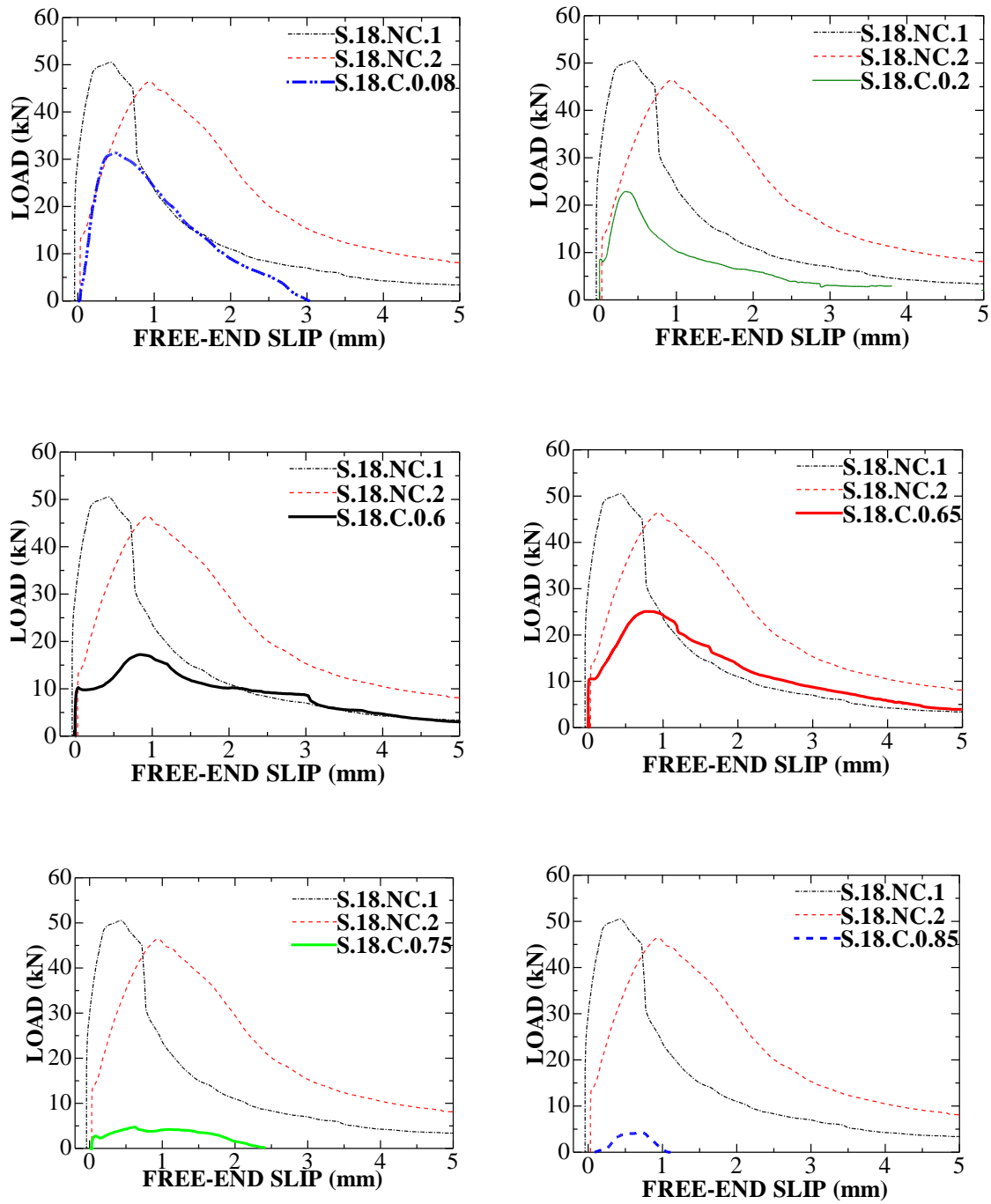


**Fig. 4.11 Pull-out load versus slip at free-end for 18 MPa specimens**

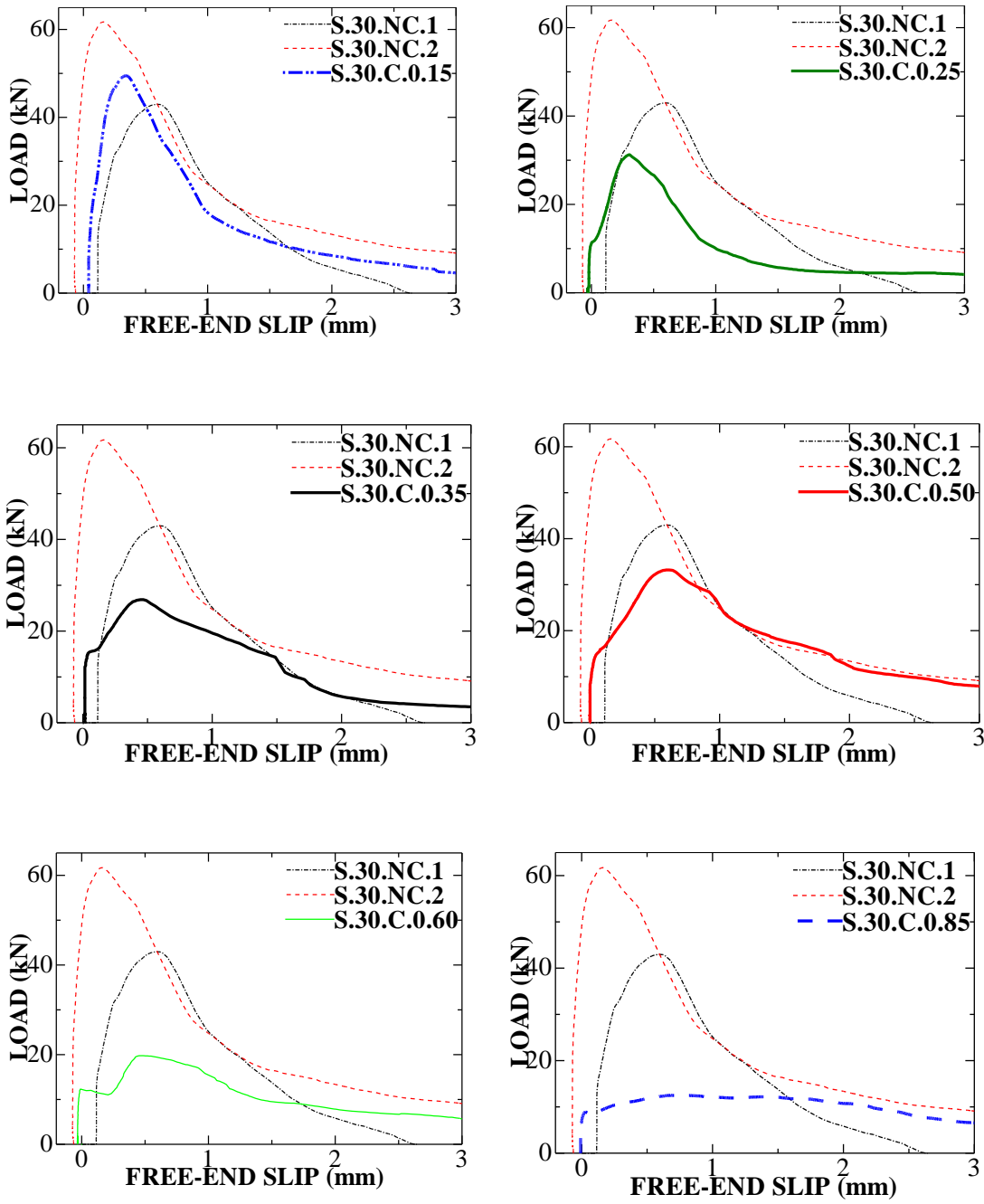


**Fig. 4.12 Pull-out load versus slip at free-end for 30 MPa specimens**

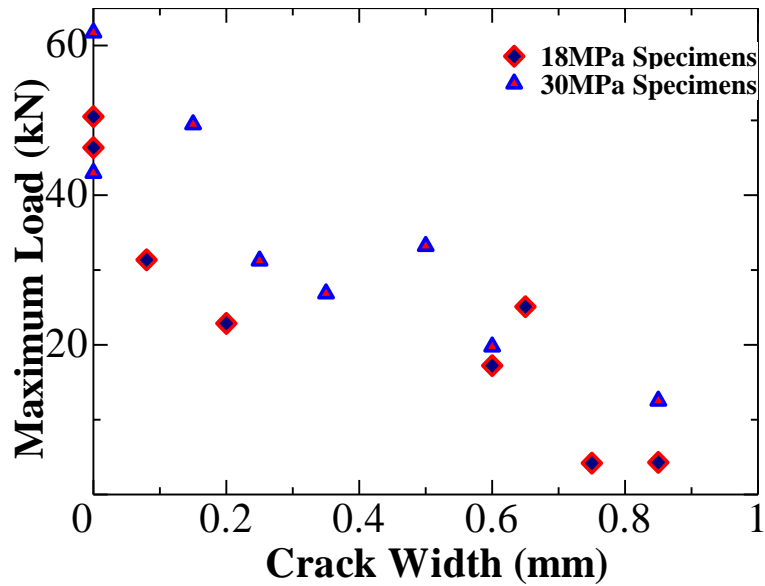


Fig. 4.13 Maximum pull-out load versus crack width before loading

#### 4.3.1.2. Crack opening versus slip

The Crack opening versus slip is plotted in Fig.4.14. The crack opening is measured by displacement transducers without including crack width before loading. In the case of plural cracks, crack opening shows the summation of the width of cracks that occurred in the gauge length of displacement transducers. With increasing of slip, the opening seems to start earlier and develop faster in case of side-splitting without new crack. In the case of an apparition of new cracks, the opening of the crack is fastest and reaches the highest value compared to other specimens. However, in some specimens, no evidence was found.

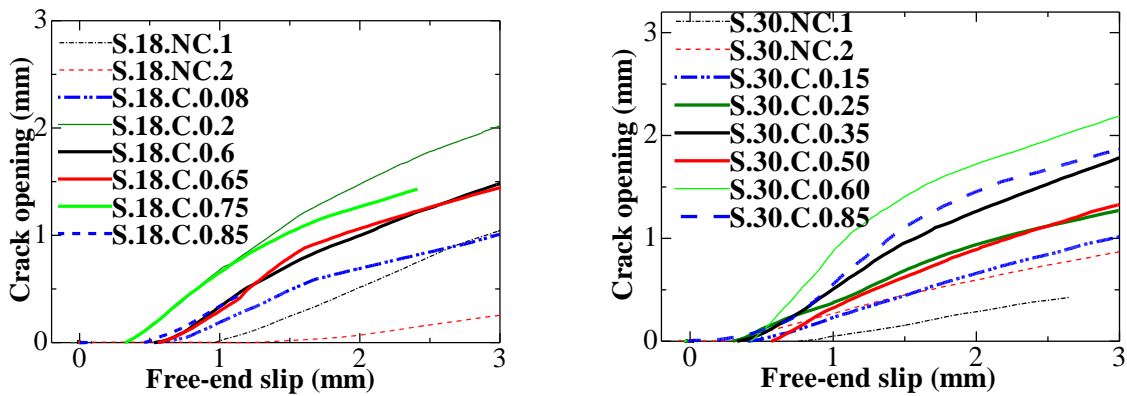


Fig. 4.14 Crack opening versus slip

#### 4.4. Bond strength degradation

##### 4.4.1. Comparison of the results with the fib model code 2010 and JCI 1998

The proposed relationship in the fib Model Code is compared with the test results in Fig. 4.15. The prediction with Model Code 2010 is in good agreement with S.30.C.0.25 and S.30.C.0.30. However, for other specimens, our results are overestimated or underestimated for 18 MPa specimens. It should be noted again that the authors of the fib model code 2010 assume that the residual strength of concrete structures is also affected by cross-section loss of steel.

In addition to that, Japan Concrete Institute in the concrete structure rehabilitation research committee reports 1998 gave an evaluation formula of the bond degradation as a function of corrosion.

$$\tau_{cor} = \exp(-3.55I \times W_{cr}) \cdot \tau_{non-cor}$$

The prediction with Japan Concrete Institute 1998 is in good agreement with S.18.C.0.08, S.18.C.0.2, S.18.C.0.75 and S.18.C.0.85. However, our results are overestimated for 30 MPa specimens.

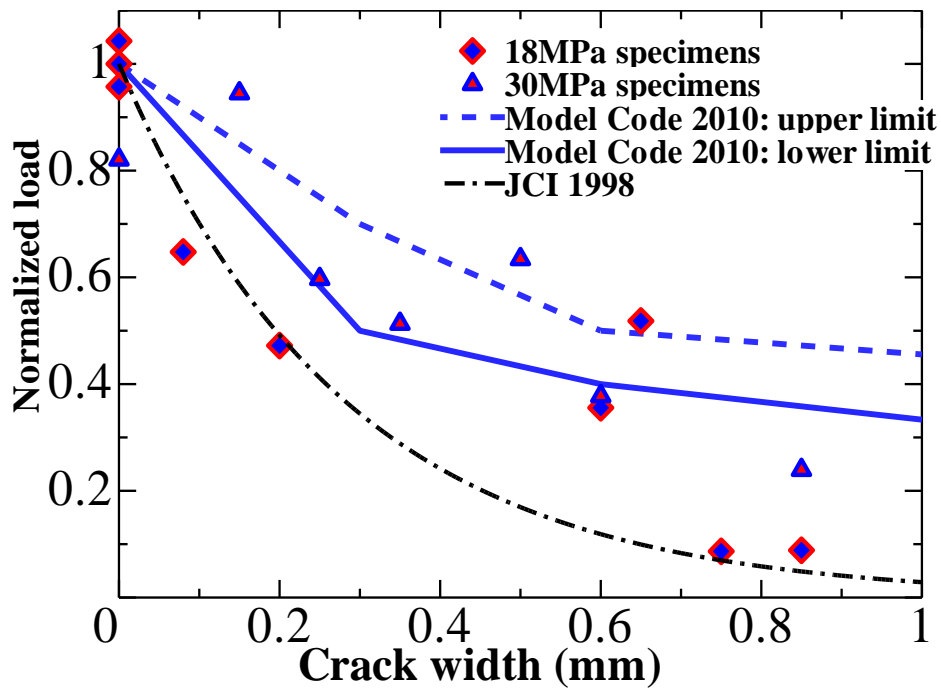


Fig. 4.15 Comparison with fib model 2010 and JCI 1998

#### 4.4.1. Bond degradation and surface crack width relationship

A simple formula for the bond strength with surface crack width as a variable is studied similarly as Chap.3.

As can be seen from the results of regression analysis in Table 4.7, an exponential equation provides the best fit (higher R<sup>2</sup>). Therefore, the following equation can be used for the prediction of the maximum pull-out load:

$$P_{(W_{cr})} = P_0 \cdot e^{-0.206W_{cr}}$$

where  $P_{(W_{cr})}$ : Pull-out strength in cracked concrete;  $P_0$ : Pull-out strength of specimen without crack;  $W_{cr}$ : Crack width.

Fig 4.16 shows the experimental result and the prediction model comparison. The ratios of the experimental to calculated values are close to one, which indicates that the concrete crack width can potentially be a good indicator to characterize bond strength degradation.

In Chap 3, a formula expressing the deterioration of the bond obtained with single splitting type specimens has been proposed. In Fig.4.16, that formula is compared to the one obtained in this chapter. It can be seen that the deterioration of the bond due to the induced cracks is more severe in a side-splitting specimen than in single-splitting specimen. This result may be explained by the fact that the number and position of induced crack can heavily affect the deterioration of the bond.

Table 4.7 Regression analysis result

Analysis	Equations	R <sup>2</sup>
<i>Linear</i>	$-0.103W_{cr}+1$	0.71
<i>Logarithmic</i>	$-0.24(W_{cr}) + 0.23$	0.62
<i>Exponential</i>	$e^{-2.06 W_{cr}}$	0.82

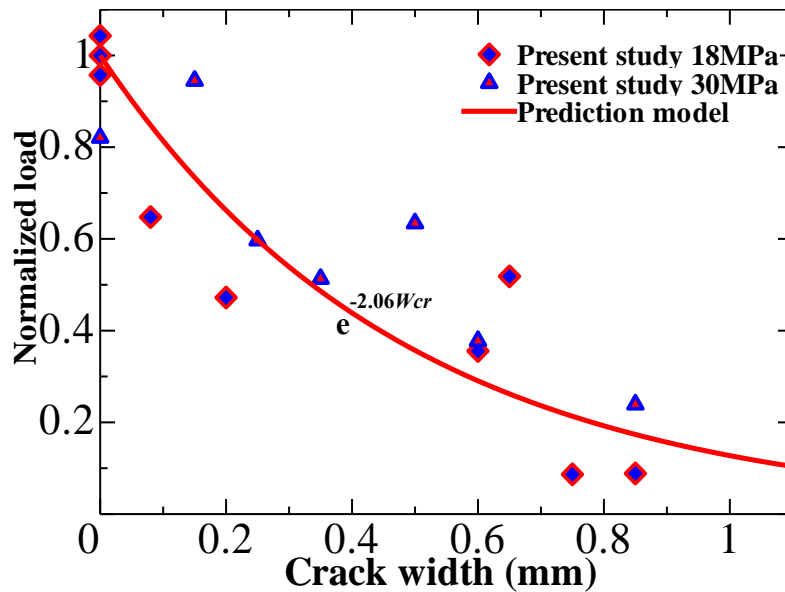
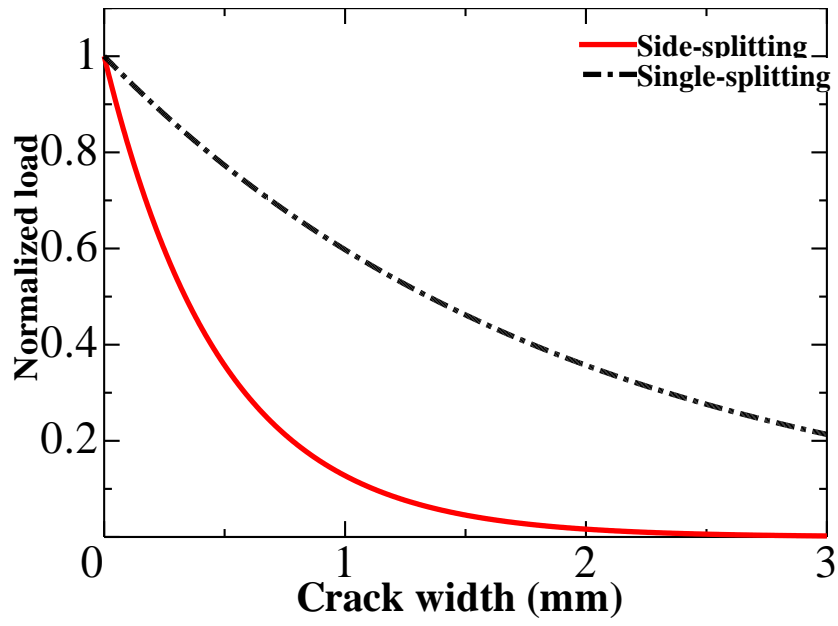


Fig. 4.16 Result and prediction model



**Fig. 4.17** Proposed evaluation formula from test result

#### **4.5. Conclusions**

In this chapter, the pull-out test is conducted on 16 concrete blocks with embedded D19 rebar following different corrosion crack width simulated by 2 EAFPs. The test is carried out on a side split type specimen. In summary, these results show that there was a significant exponential correlation between pull-out strength and surface crack width. Also, a simple formula to predict bond degradation is proposed by using the surface crack width as the main variable.

The prediction with Model Code 2010 is in good agreement only with S.30.C.0.25 and S.30.C.0.30.

The prediction with Japan Concrete Institute 1998 is in good agreement with S.18.C.0.08, S.18.C.0.2, S.18.C.0.75 and S.18.C.0.85. However, our results are overestimated for 30 MPa specimens.

A comparison of the two results (single splitting and side splitting) reveals that the deterioration of the bond due to the induced cracks was more severe in a side-splitting specimen than in single-splitting specimen.

## Chapter 5 Conclusions

The present study deals with the relationship between the bond strength of corroded steel bars and the surface crack width. A total of 28 specimens were subjected to pull-out test. On the basis of the experimental evidence and discussions presented in this thesis, the following remarks can be drawn:

- 1) The expansion agent filled pipe is a promising method that allows focussing in the cracking itself. The tensile test shows that the strain in the axis, top and between the ribs tended to increase over the time after the filling of the expansion agent. In addition, at the beginning of the loading, with the increasing of the axial strain, the yield strength and modulus of elasticity of the pipe filled with an expansion agent also increase. However, the elongation at failure tended to decrease. The tensile strength was not affected.
- 2) The specimens were categorized in: “Single-split type” when the induced cracks are along the rebar and “Side split-type” when the induced cracks are located on the surroundings and perpendicular to the rebar. All specimens experienced failure due to splitting. A group of specimens failed by newly generated splitting crack despite existing induced crack and other specimens failed by the opening of the induced crack.
- 3) There was a significant correlation between residual bond strength and induced crack width. This demonstrates that the surface crack width can potentially be a good indicator to evaluate the bond strength degradation.
- 4) The decrease of the pull-out load is more severe in 18MPa specimens than in 30 MPa specimens.
- 5) The deterioration of the bond due to the induced cracks was more severe in a “Side-split type” than in “Single split-type”.
- 6) Empirical models, which relate the bond deterioration with the longitudinal cracks and the lateral cracks have been proposed. However, more research is necessary to investigate the influence of other involved parameters (e.g. cover/diameter ratio, confinement, bar profile) to develop a predictive model for general applicability.

## DEDICACES

The work presented in this master thesis represents two years of study and research at the University of Tsukuba.

The present work was carried out between April 2018 and March 2020 in the Kanakubo lab.

This was possible thanks to the scholarship received from the Japanese Government Scholarship, funded by the Ministry of Education, Culture, Sports, Science and Technology (MEXT). I am very appreciative for giving me this opportunity.

First of all, I would like to express my most sincere gratitude to my supervisor, Prof. Kanakubo Toshiyuki. Throughout my journey in Japan, he has shared his vast knowledge and experience, providing valuable discussion, advice and insights yet he has always given me the freedom to conduct my own research, allowing me to evolve. Given his level of commitment to my research, his understanding and his thorough review of my work, I cannot think of anyone better to have as supervisor. Also, a big thanks to his wife, Kanakubo Noriko, for being a valuable advisor during my life in Japan.

I want to convey my appreciation to my vice-supervisor, Prof. Yasojima Akira and Prof. Shoji Gaku, for showing their interest in my work and taking the time to get involved and share their valuable thoughts, comments and also having their door always open to share their vast knowledge.

I would also like to thank all my colleagues, former and present, at Kanakubo laboratory for creating such a nice working environment. Special thanks go to Aburano Togo and Kojima Atsushi for their help in executing all the experimental work.

Finally, I want to direct my special thanks to my lovely family, my wife Aida, who has been very understanding and patient during my study. Their love and affection have been indispensable in this journey and none of this would have been possible without their unconditional support. For all that and much more, thank you.

## REFERENCES

- [1] R. Tefers, Cracking of concrete cover along rebars, Mag. Concr. Res. 31(106) (1976) 3-12
- [2] fib Bulletin No. 10. (Bond of reinforcement in concrete 2000)
- [3] Rodriguez et al.: Corrosion of reinforcing bars and service life of reinforced concrete structures: corrosion and bond deterioration. Int. Conf. on Concrete across Borders, Odense, Denmark, Vol. II, pp 315-326, 1994
- [4] Auyeung et al: Bond-behavior of corroded reinforcement bars. ACI Structural Journal 97(2):214-220,2000
- [5] Al-Sulaimani et al.: Influence of corrosion and cracking on bond behavior and strength of reinforced concrete. Proceedings American Concrete Institute, Vol 87, No.2, Mar-Apr. pp220-231 ,1990
- [6] fib Model Code 2010, Vol.1. International Federation for Structural Concrete, Lausanne, Switzerland.
- [7] SYLL, A. S., Kawamura, Y., Kanakubo, T.: Simulation of Concrete Cracks due to Bar Corrosion by Aluminum Pipe Filled with An Expansion Agent, Summaries of Technical Papers of Annual Meeting, Architectural Institute of Japan, Structure IV, pp.55-56, 2018.9
- [8] Yasojima, A., Kanakubo, T., Bond Splitting Strength of RC Members Based on Local Bond Stress and Slip Behavior, 11th International Conference on Fracture, No.4486, 2005.
- [9] Yang, Y., Nakamura, H., Miura, T., Yamamoto, Y., Effect of corrosion-induced crack and corroded rebar shape on bond behavior, Proceedings of the Japan Concrete Institute, Vol. 40, No. 1, pp.927-932, 2019.